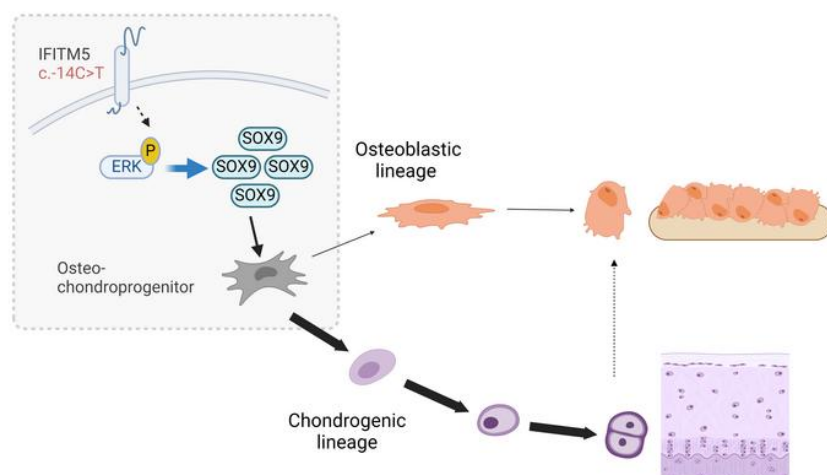# The *IFITM5* mutation in osteogenesis imperfecta type V is associated with an ERK/SOX9-dependent osteoprogenitor differentiation defect

Ronit Marom, … , Jason D. Heaney, Brendan H. Lee

Research | In-Press Preview | Bone biology | Genetics

Graphical abstract

The *IFITM5* mutation in osteogenesis imperfecta type V is associated with an ERK/SOX9-dependent osteoprogenitor differentiation defect

Ronit Marom[1,2*], I-Wen Song[1], Emily C. Busse[1,3], Megan E. Washington[1], Ava S. Berrier[1], Vittoria C. Rossi[1,2], Laura Ortinau[1], Youngjae Jeong[1], Ming-Ming Jiang[1], Brian C. Dawson[1], Mary Adeyeye[1], Carolina Leynes[1], Caressa D. Lietman[1†], Bridget M. Stroup[1], Dominyka Batkovskyte[1‡], Mahim Jain[1], Yuqing Chen[1], Racel Cela[1], Alexis Castellon[1], Alyssa A. Tran[1], Isabelle Lorenzo[1], D. Nicole Meyers[4], Shixia Huang[5], Alicia Turner[1,2], Vinitha Shenava[6], Maegen Wallace[7§], Eric Orwoll[8], Dongsu Park[1], Catherine G. Ambrose[4], Sandesh C.S. Nagamani[1,2], Jason D. Heaney[1] and Brendan H. Lee[1,2*]

Affiliations:

[1]Department of Molecular and Human Genetics, Baylor College of Medicine, Houston TX, 77030 USA

[2]Texas Children's Hospital, Houston TX, 77030 USA

[3]Medical Scientist Training Program, Baylor College of Medicine, Houston TX, 77030 USA

[4]Department of Orthopaedic Surgery, McGovern Medical School at UT Health, Houston TX, 77030 USA

[5]Department of Molecular and Cellular Biology, and Department of Education, Innovation, and Technology, Advanced Technology Cores, Baylor College of Medicine, Houston TX, 77030 USA

[6]Department of Orthopedic Surgery, Baylor College of Medicine, Houston TX, 77030 USA

[7]Orthopaedic Surgery, University of Nebraska Medical Center, Children's Hospital and Medical Center, Omaha NE, 68114 USA

[8]Department of Medicine, Bone and Mineral Unit, Oregon Health & Science University, Portland OR, 97239 USA

† CDL present affiliation: Department of Pathology, Microbiology and Immunology, Vanderbilt University Medical Center, Nashville TN, USA

‡ DB present affiliation: Department of Molecular Medicine and Surgery, Karolinska Institutet, Stockholm, 17177 Sweden

§ MW present affiliation: Phoenix Children's Hospital, University of Arizona, Phoenix AZ, USA

*To whom correspondence should be addressed:

Brendan Lee, M.D., Ph.D.
Department of Molecular and Human Genetics
Baylor College of Medicine
One Baylor Plaza, Room R814

1   Houston, TX 77030
2   Fax number: 713-798-5168
3   Telephone number: 713-798-8853
4   Email: blee@bcm.edu
5
6   Ronit Marom, M.D., Ph.D.
7   Department of Molecular and Human Genetics
8   Baylor College of Medicine
9   One Baylor Plaza, Room R803
10   Houston, TX 77030
11   Fax number: 713-798-5168
12   Telephone number: 713-798-4523
13   Email: ronit.marom@bcm.edu
14
15

16   **The authors have declared that no conflict of interest exists.**

17

18

19

20

21

22

23

24

25

26

27

28

29

30

31

32

33

34

35

ABSTRACT

Osteogenesis imperfecta (OI) type V is the second most common form of OI, distinguished by hyperplastic callus formation and calcification of the interosseous membranes in addition to bone fragility. It is caused by a recurrent, dominant pathogenic variant (c.-14C>T) in *IFITM5*. Here, we generated a conditional *Rosa26* knock-in mouse model to study the mechanistic consequences of the recurrent mutation. Expression of the mutant *Ifitm5* in osteo-chondroprogenitor or chondrogenic cells resulted in low bone mass and growth retardation. Mutant limbs showed impaired endochondral ossification, cartilage overgrowth, and abnormal growth plate architecture. The cartilage phenotype correlates with the pathology reported in OI type V patients. Surprisingly, expression of mutant *Ifitm5* in mature osteoblasts caused no obvious skeletal abnormalities. In contrast, earlier expression in osteo-chondroprogenitors was associated with increase in the skeletal progenitor population within the periosteum. Lineage tracing showed that chondrogenic cells expressing the mutant *Ifitm5* showed decreased differentiation into osteoblastic cells in diaphyseal bone. Moreover, mutant IFITM5 disrupts early skeletal homeostasis in part by activating ERK signaling and downstream SOX9 protein, and inhibition of these pathways partially rescued the phenotype in mutant animals. These data identify the contribution of a signaling defect altering osteo-chondroprogenitor differentiation as a driver in the pathogenesis of OI type V.

1 **INTRODUCTION**

2   Osteogenesis imperfecta (OI) is an inherited multi-systemic disorder characterized by low

3 bone mass, recurrent fractures, growth deficiency and skeletal deformities (1-3). Extra-skeletal

4 manifestations may include muscle weakness, dentinogenesis imperfecta, hearing loss, and

5 pulmonary disease (1-3). OI is genetically and phenotypically heterogenous. Most OI (~85%) is

6 caused by pathogenic variants in *COL1A1* or *COL1A2* which encode alpha 1 and alpha 2 chains

7 of type I collagen, respectively, while the remainder are caused by pathogenic variants in genes

8 involved in collagen processing, or in the regulation of bone homeostasis (1, 3, 4). OI type V is

9 the most common type of OI that is not caused by alterations in type I collagen and is estimated

10 to account for up to 9-10 percent of moderate-severe OI (5-7). Clinically, OI type V is

11 characterized by the unique features of hyperplastic callus formation (which can occur with or

12 without a fracture), and calcification of the interosseous membranes, in addition to the bone

13 fragility (8). Notably, all individuals with OI type V have the same autosomal dominant

14 pathogenic variant (c.-14C>T) in *IFITM5 (9-12)*. This variant resides in the 5' untranslated

15 region (UTR) and introduces a new in-frame start codon, adding 5 amino acid residues at the N

16 terminus of the protein (13). *IFITM5* encodes the interferon inducible transmembrane protein 5

17 (also known as BRIL), a member of the highly conserved IFITM (interferon-induced-

18 transmembrane) family of proteins that are implicated in innate immune response (9-12, 14).

19 Unlike other IFITM proteins that are expressed ubiquitously, *IFITM5* is primarily expressed in

20 skeletal tissues, in osteoblasts (15, 16), chondrocytes (9, 15, 17), and progenitor niches like the

21 groove of Ranvier (9). Studies suggest that it has a role in bone mineralization (15) but does not

22 exhibit anti-viral activity or other function related to the immune system, as observed with other

23 IFITM proteins (18).

1   The molecular consequences of the recurrent (c.-14C>T) OI type V pathogenic variant

2   remain unknown. Expression of the mutant *Ifitm5* allele in transgenic mice overexpressing the

3   mutant protein in bone, and in CRISPR/Cas9 knock-in mouse models, both resulted in a severe

4   OI phenotype with perinatal lethality (19-21). Importantly, overexpression of wild type *Ifitm5*

5   and complete loss-of-function models showed no obvious phenotypes (16, 19). Thus, a

6   *neomorphic* effect in bone has been suggested as the most likely mechanism. However, the

7   cellular and signaling mechanisms by which the mutant IFITM5 drives the skeletal pathology is

8   not understood. Here, we report a conditional *Rosa26* mutant *Ifitm5* knock-in mouse model that

9   is viable and recapitulates the human phenotype, thus facilitating the understanding of the role of

10   the mutant protein in specific stages of osteoblast and chondrocyte differentiation. Findings in

11   this model, supported by studies in the previously reported transgenic *Ifitm5$^{c.-14C>T}$* mice (19), as

12   well as in zebrafish and *in vitro* cell culture models, point to downstream activation of ERK

13   (Extracellular signal-Regulated Kinase)/MAPK (Mitogen-Activated Protein Kinase) signaling

14   and increased SOX9 protein leading to the abnormal osteo-chondroprogenitor differentiation in

15   OI type V pathogenesis.

16

17

18

19

20

21

22

23

1   **RESULTS**

2   *Conditional expression of the mutant Ifitm5$^{c.-14C>T}$ allele in limb mesenchyme*

3   *(Rosa26^{mIfitm5};**Prx1-Cre***), but not in mature osteoblasts (Rosa26^{mIfitm5};**OC-Cre***), results in low*

4   *bone mass.*

5   All mouse models generated to date for OI type V exhibit perinatal lethality. Therefore,

6   we generated a conditional mouse expressing the disease-causing *IFITM5* mutation at specific

7   stages of osteoblast and chondrocyte cell differentiation. We inserted the mutant *Ifitm5$^{c.-14C>T}$*

8   allele (m*Ifitm5*) into the *Rosa26* locus (22) via homologous recombination (**Fig. 1A, B**). To study

9   whether the human OI type V phenotype is recapitulated in this model, we crossed mice that are

10   heterozygous for the *Rosa26* knock-in m*Ifitm5* allele (*Rosa26$^{mIfitm5/+}$*) with: 1) Paired related

11   homeobox 1 (Prx1-Cre) transgenic mice that express the Cre-recombinase (Cre/-) in

12   mesenchymal precursors of the osteo-chondroprogenitor lineage, and 2) Osteocalcin-Cre (OC-

13   Cre) transgenic mice that express the Cre-recombinase (Cre/-) in mature osteoblasts. Controls

14   included littermates that expressed only Cre-recombinase (Cre/-), that carried only the *Rosa26*

15   knock-in allele (*Rosa26$^{mIfitm5/+}$*), or that carried neither allele (*Rosa26$^{+/+}$*). The activation of *Cre*

16   recombinase was validated by PCR using primers spanning the deleted *LoxP* cassette, and by

17   quantitative RT-PCR showing expression of the mutant *Ifitm5* mRNA in bone (**Fig. S1**).

18   At age 2 months, trabecular bone volume (BV/TV), as measured by micro CT in distal

19   femurs, was significantly reduced in the *Rosa26^{mIfitm5}*;Prx1-Cre mice in both males (**Fig. 2A**) and

20   females (**Fig. S2**). Consistent with this finding, trabecular number was decreased and trabecular

21   spacing was increased in *Rosa26^{mIfitm5}*;Prx1-Cre mice compared to littermate controls. Cortical

22   thickness was not significantly affected, but histological sections showed immature bone, as is

23   seen in bone histology from a patient with OI type V (**Fig. 2B**), and consistent with previous

1 reports (8). Interestingly, expression of the mutant *Ifitm5* allele in mature osteoblasts in the

2 Rosa*26^{mIfitm5}*;OC-Cre mice did not have an obvious effect on bone mass in mutant mice

3 (*Rosa26^{mIfitm5/+}*;OC-Cre/-) compared with controls (**Fig.2C and Fig. S3**). We further studied the

4 effect of mutant *Ifitm5* expression in committed, early-differentiating osteoblasts via the 2.3 kb

5 rat Col1a1-Cre promoter (*Rosa26^{mIfitm5}*;Col1a1-Cre). In this model, the bone mass in mutant

6 animals was not significantly different than Cre controls (**Fig. S4**). The divergent observations,

7 in *Rosa26^{mIfitm5}*;OC-Cre and *Rosa26^{mIfitm5}*;Col1a1-Cre vs. *Rosa26^{mIfitm5}*;Prx1-Cre mouse models,

8 represent the consequences of distinct temporo-spatial expression of the mutant protein and

9 suggest an early developmental effect in osteo-chondroprogenitors, and that its expression in

10 committed and mature osteoblasts is not a major contributor to the bone phenotype.

11

12 ***Conditional expression of the mutant Ifitm5 allele results in abnormal cartilage development,***

13 ***leading to growth restriction and progressive joint deformity in Rosa26^{mIfitm5};Prx1-Cre mice.***

14   *Rosa26^{mIfitm5}*;Prx1-Cre mutant mice showed reduced weight gain, and significantly

15 shortened femurs as compared to littermate controls (**Fig. 3A, B** and **Fig. S2**). Histological

16 sections of the tibial proximal growth plate at P.14 showed disorganization of the columnar

17 structure of the proliferative and hypertrophic zones in the mutant mice. Most notably, the

18 hypertrophic zone was reduced, as demonstrated by immunohistochemistry staining for type X

19 collagen, a marker of hypertrophic chondrocytes (**Fig. 3C, D**).

20   Studies have shown that *Prx1*-expressing cells in the periosteum serve as a reservoir for

21 osteo-chondroprogenitor cells during bone development and fracture healing (23, 24). Therefore,

22 we next tested whether shortened femurs in the *Rosa26^{mIfitm5}*;Prx1-Cre mutant mice are due to

23 the defect of periosteal progenitor cell population or due to the defect of their differentiation. We

1   performed flow cytometry analysis of periosteal skeletal progenitors by negative selection for

2   hematopoietic (CD45), endothelial (CD31) and erythroid (Ter119) lineage markers, and positive

3   selection for CD105 and CD140a (25). Notably, this analysis demonstrated a significant increase

4   in the percentage of periosteal CD45$^-$CD31$^-$Ter119$^-$CD105$^+$CD140a$^+$ population in

5   *Rosa26^{mIfitm5}*;Prx1-Cre mutant mice (5.07 %) compared to littermate controls (2.55 %) (**Fig.**

6   **4A,B**), whereas skeletal progenitor cell population in the bone marrow was not different (**Fig. 4B**

7   and **Fig. S5**). These data further support the impact of the OI type V mutation on skeletal

8   progenitors as a potential driver of the phenotype.

9   Skeletal preparations at P.21 showed irregular structure of the proximal long bones, with

10   cartilaginous material accumulating in periarticular tissues (**Fig. 5A** and **Fig. S6**). At age 2

11   months, skeletal radiographs revealed partial joint ossification, leading to joint deformities and

12   contractures at the knees and ankles (**Fig. 5B**). Histology revealed progression of the abnormal

13   growth plate ultrastructure, with cartilage overgrowth and disruption of the endochondral

14   ossification at the proximal tibial metaphysis (**Fig. 5C**). In contrast, growth was not significantly

15   altered in the *Rosa26$^{mIfitm5/+}$*;OC-Cre/- or in *Rosa26$^{mIfitm5/+}$*;Col1a1-Cre/- mice that express the

16   mutant allele in more mature osteoblasts (**Fig. S3 and Fig. S4**).

17

18   ***Increased ERK signaling contributes to abnormal skeletal phenotype in OI type V models***.

19   To study the molecular consequences of the IFITM5 mutation in bone, we performed a

20   proteomic analysis in calvaria of our previously reported transgenic mouse model that

21   constitutionally overexpressed the mutant *Ifitm5* from the *Col1a1* 2.3kb promoter *(19)*. Reverse

22   Phase Protein Array (RPPA) analysis detected elevated ERK1/2 phosphorylation (**Fig. 6A, B**).

23   This correlated with immunohistochemistry staining for phosphorylated ERK in

1   *Rosa*26^{mIfitm5};Prx1-Cre mice, that showed abundant positive staining in chondrocytes adjacent to

2   the ossification centers at the proximal tibia (**Fig. S7**). To understand the functional

3   consequences of increased ERK activation, we then generated an *in vitro* cell culture model of

4   OI type V that stably overexpresses the mutant *Ifitm5* in MC3T3 cells under doxycycline

5   induction. Consistent with the observations in OI type V mouse models, expression of mutant

6   IFITM5 in MC3T3 cells was associated with increased ERK phosphorylation and delayed

7   mineralization *in vitro* (**Fig. S7**). The delayed mineralization observed in this cell model was

8   consistent with the effect on cultured calvarial osteoblasts in the previously published OI type V

9   mouse models (19, 20). Importantly, treatment with the ERK inhibitor U0126 restored

10   mineralization in MC3T3 *mIfitm5* mutant cells in a dose-dependent manner (**Fig. S7**).

11   To test the relationship between ERK activation and abnormal cartilage formation in OI

12   type V, we generated a zebrafish (*Danio rerio*) model of OI type V and performed *in vivo* rescue

13   experiments. Mutant *IFITM5* mRNA was injected to zebrafish embryos at the one cell stage [30

14   minutes to 1 hour post fertilization (*hpf*)]. Subsequently, 34% of the embryos at 5 days post

15   fertilization (*dpf*) showed abnormal morphology (abnormal craniofacial cartilage development

16   and curved/kinked tail), compared to only 5-10% in control groups that were injected with either

17   wild type IFITM5, or mCherry mRNA (**Fig. 6C,D**). Treatment with the pharmacologic

18   MEK/ERK inhibitor PD0325901 significantly increased the proportion of IFITM5 mutant

19   zebrafish that survived with typical development by 18% at 5 *dpf* (**Fig. 6D**).

20

21   ***Altered spatio-temporal expression of SOX9 impairs chondrogenic maturation and disrupts***

22   ***endochondral bone formation in OI type V models***.

1   The RPPA analysis also detected increased level of SOX9, a master regulator of cartilage

2   development, in protein extracted from the mutant transgenic mice calvaria (**Fig. 7A, B**).

3   Therefore, we studied the expression of SOX9 in the conditional $Rosa26^{mIfitm5}$;Prx1-Cre mutant

4   mice that showed disruption of the growth plate structure and cartilage overgrowth (**Fig. 3, 5**).

5   Immunohistochemistry for SOX9 in proximal tibia sections at P.14 identified increased staining

6   intensity and altered spatial distribution of SOX9-positive cells in the growth plate, with

7   persistence of SOX9 staining in hypertrophic chondrocytes (**Fig. 7C**). Notably, western blot

8   analysis in ATDC5 chondrogenic cells demonstrated that wild type IFITM5 was co-induced with

9   SOX9 expression during chondrogenic differentiation (**Fig. S8**).

10   Prx1-Cre transgenic mice express the *Cre* recombinase in mesenchymal cells that

11   differentiate to osteogenic and chondrogenic lineages. As mature osteoblastic lineage expression

12   of mutant IFITM5 did not lead to abnormal skeletal phenotype, we explored whether cartilage-

13   specific expression was sufficient to cause the skeletal phenotype. Thus, we studied the effect of

14   postnatal activation of the mutant *Ifitm5* allele in chondrocytes via inducible $Rosa26^{mIfitm5}$;*Acan-*

15   *Cre ERT2* mice. Similar to the findings in the Prx1-Cre mouse model, expression of mutant

16   *Ifitm5* in chondrocytes under Aggrecan promoter at P.10 disrupted the growth plate architecture,

17   leading to disorganized columnar structure and reduced hypertrophic zone, as shown by H&E

18   staining and SOX9 immunohistochemistry (**Fig. 8A,B**). Immunohistochemistry staining showed

19   altered spatio-temporal expression of SOX9 and type X collagen in the mutant samples (**Fig.**

20   **8B,C**). Not surprisingly, $Rosa26^{mIfitm5}$;*Acan-Cre ERT2* mutant mice exhibited a milder, but

21   significant growth defect and low bone mass, phenocopying the $Rosa26^{mIfitm5}$; Prx1-Cre mice

22   (**Fig.8D,E**). Moreover, biomechanical testing via 3-point bending showed reduced ductility and

23   increased bone stiffness in the $Rosa26^{mIfitm5}$;*Acan-Cre ERT2* mutant mice (**Fig. S9**). To evaluate

1   whether increased SOX9 is a driver of the skeletal phenotype, we intercrossed the

2   *Rosa*26^{mIfitm5};*Acan-Cre ERT2* mice to *Sox9^{flox}* mice. Postnatal genetic deletion of *Sox9* in cells

3   expressing the mutant IFITM5 significantly improved the growth plate architecture, as shown by

4   H&E staining, and by immunohistochemistry for SOX9 and type X collagen (**Fig. 8A-C**).

5   Furthermore, micro CT analysis demonstrated partial rescue of the growth restriction and low

6   bone mass phenotype in *Rosa*26^{mIfitm5};*Sox9$^{fl/+}$*;*Acan-Cre ERT2* mice (**Fig. 8E**).

7

8   *OI type V is an osteochondrodysplasia*.

9   The OI type V mouse models reported here recapitulate, at least in part, the human

10   phenotype by exhibiting low bone mass, expansile cartilage formation, and growth restriction (9,

11   10). They exhibit similar histologic and radiographic features to those reported in the human

12   patients (8), including immature bone matrix with mesh-like appearance (**Fig. 2B**) and sclerotic

13   bands in the femur metaphysis (**Fig. 5B**). Additionally, *Rosa26^{mIfitm5}*;Prx1-Cre mice demonstrate

14   joint deformities. To correlate this finding with the human phenotype, we performed a

15   retrospective chart review of seven individuals with OI type V from 3 skeletal centers in the

16   United States and identified variable degree of joint dysfunction in six of the seven participants

17   (85%, **Fig. S11 and Table S1**). Taken together, our data suggest that mutant IFITM5 expression

18   leads to abnormal chondrogenesis while inhibiting osteo-chondroprogenitor cells' maturation

19   into bone. To support this hypothesis, we crossed the *Rosa26^{mIfitm5}*;*Acan-Cre ERT2* mice with

20   Ai9 reporter mice (B6.Cg-*Gt(ROSA)26Sor$^{tm9(CAG-tdTomato)Hze}$*/J), and traced reporter-positive cells

21   3 weeks following post-natal activation of the mutant *Ifitm5* allele. In *Rosa26$^{mIfimt5/Ai9}$*;*Acan-Cre*

22   *ERT2* mice, cells co-expressing the Ai9 reporter and mutant *Ifitm5* showed altered distribution

23   with retention in the growth plate area and decreased migration to the femur shaft (**Fig. 9 A-B**),

1   consistent with decreased differentiation into osteoblasts, whereas in littermates controls *Acan-*

2   *Cre ERT2*^{+} cells marked with Ai9 reporter showed the expected pattern of migration along the

3   diaphysis (26). Next, we performed total RNA sequencing in *Rosa*26*[mIfitm5]*;*Acan-Cre ERT2*

4   mouse femurs to search for downstream transcriptomic changes in the long bones following

5   activation of the mutant *Ifitm5* allele in chondrocytes. GO enrichment analysis in mutant femurs

6   revealed enrichment for chondrocyte morphogenesis, proliferation, and differentiation processes

7   (**Fig. 9C**). A focused differential gene expression analysis demonstrated up-regulation of

8   chondrogenic markers and down-regulation of osteoblast markers (**Fig. 9D**). Consistent with this

9   observation, activation of the mutant *Ifitm5* allele in cultured marrow stromal cells via soluble

10   Cre recombinase was associated with decreased osteoblastic differentiation and enhanced cell

11   condensation towards chondrogenic differentiation *in vitro* (**Fig. S12**).

12

13

14

15

16

17

18

19

20

21

22

23

24

25

26

27

DISCUSSION

OI type V is one of the more common causes of moderate to severe OI, second only to collagen I related forms (5-7). The pathogenic mechanism in OI type V is unknown, hindering the development of efficient and targeted therapies. We have previously generated a transgenic mouse model by overexpressing *Ifitm5* cDNA with the novel start codon, corresponding to the recurrent human OI type V mutation, under the control of the *Col1a1* 2.3 kb promoter (19). The mutant *Ifitm5* transgenic mice exhibited perinatal lethality and severe bone deformities while transgenic mice overexpressing wild type *Ifitm5* did not show significant abnormalities (19). Consistent with our transgenic mouse model, others subsequently published a CRISPR/Cas9 knock-in mouse model that also exhibited a severe OI phenotype with perinatal lethality (20, 21), suggesting that a conditional, tissue and stage-specific expression of the mutant *Ifitm5* may be an effective approach for mechanistic analyses. We report here the first conditional mouse model for OI type V that expresses mutant IFITM5 in three different cell types, i.e., limb mesenchymal cells, osteogenic cells, and chondrogenic cell lineages. Mice expressing the mutant *Ifitm5* allele are viable and recapitulate the low bone mass and exuberant cartilage formation that is observed in humans with OI type V.

The phenotypic similarity and overlapping severity between the *Rosa26^{mIfitm5}*;Prx1-Cre and *Rosa26^{mIfitm5}*;*Acan-Cre ERT2* mice support that abnormal chondrogenesis is a major contributor to the skeletal phenotype. The expression of *IFITM5* in cartilage has been demonstrated in humans and mice (9, 15). Transcriptomic analysis has shown enrichment of *IFITM5* mRNA during chondrogenesis in human bone marrow mesenchymal cells (17), and in developing chick embryos (27). We confirmed this finding by showing that expression of the IFITM5 is upregulated in conjunction with SOX9 in differentiating chondrogenic ATDC5 cells

1   (**Fig. S8**). In *Rosa26^{mIfitm5}*;Prx1-Cre mice, expression of the mutant *Ifitm5* in mesenchymal

2   progenitors of the osteo-chondrogenic lineage was associated with low bone mass and growth

3   restriction, while the *Rosa26^{mIfitm5}*;Col1a1-Cre and *Rosa26^{mIfitm5}*;OC-Cre mice that expressed the

4   mutant *Ifitm5* in committed or mature osteoblasts did not exhibit significant skeletal

5   abnormalities (**Fig. 2, 3 and Fig. S3, S4**).

6   Previously published OI type V mouse models demonstrated a severe reduction in

7   osteoblast differentiation, and replacement of the normal bone tissue with cartilaginous matrix

8   (19, 20). It is possible that the expression of the mutant IFITM5 in skeletal progenitor cells alters

9   their lineage differentiation in early development. Consistent with this hypothesis, we found that

10   the percentage of periosteal skeletal progenitor cells was significantly increased in the mutant

11   *Rosa26^{mIfitm5}*;Prx1-Cre mice (**Fig. 4A, B**)*.* Moreover, histological sections in 2 months old

12   *Rosa26^{mIfitm5}*;Prx1-Cre mice showed the failure of chondrogenic terminal differentiation and

13   impaired endochondral ossification (**Fig. 5C**). In the *Rosa26^{mIfitm5};Acan-Cre ERT2* mutant mice

14   that have an overlapping skeletal phenotype with the *Rosa26^{mIfitm5}*;Prx1-Cre model, tracing of

15   cells co-expressing the Ai9 reporter and mutant *Ifitm5* showed decreased differentiation to

16   osteoblasts, and bone transcriptome showed enrichment for chondrogenic markers expression

17   (**Fig. 9**). These data suggest that the mutant IFITM5 can maintain or induce osteo-chondro

18   progenitor numbers while inhibiting their terminal differentiation. This then can reduce the pool

19   of osteoblastic cells derived from progenitors in the growth plate (28).

20   The biochemical mechanisms whereby the mutated IFITM5 protein causes the skeletal

21   pathology in OI type V are not well-understood. Unlike other forms of OI that are associated

22   with abnormalities in type I collagen (i.e., qualitative or quantitative defects of type I collagen,

23   and abnormal processing of type I collagen), our previous transgenic mouse model failed to

1 reveal any significant change in the distribution of collagen throughout the bone or in its post-

2 translational modifications (19). Since IFITM5 forms part of a protein complex at the membrane

3 (29) and the localization of the mutant IFITM5 is not altered (30), it is possible that a

4 neomorphic effect on protein-protein interactions at the plasma membrane may alter downstream

5 signaling cascades. Proteomic analysis using RPPA identified increased levels of phosphorylated

6 ERK1/2 in the calvaria of transgenic $Ifitm5^{c.-14C>T}$ mice. Further studies in cells and zebrafish

7 overexpressing mutant IFITM5 support that activation of this pathway is involved in the

8 mineralization defect and abnormal cartilage development in OI type V (**Fig. 6 and Fig. S7**). The

9 ERK/MAPK signaling pathway has a critical role in both cartilage and bone development.

10 Previous studies have shown that this pathway may regulate osteoblast differentiation by

11 activating downstream RUNX2 and OSX-mediated transcription of osteogenic genes (31). ERK

12 signaling has been implicated in pigment epithelium derived factor (PEDF)-mediated regulation

13 of osteoblast maturation and mineralization (32). Inactivation of ERK1 and ERK2 in

14 mesenchymal osteo-chondroprogenitor cells in the $ERK1^{-/-}$; $ERK2^{flox/flox}$; Prx1-Cre mice

15 disrupted osteoblast differentiation and resulted in severe bone deformities (33). In agreement

16 with these findings, activation of MAPK signaling via transgenic overexpression of a

17 constitutively active MEK1 stimulated osteoblast differentiation and mineralization (34).

18 Conversely, somatic mosaicism for gain-of-function mutations in *MAPK2* in melorheostosis was

19 associated with increased osteoid formation and decreased mineralization *in vivo*, and impaired

20 osteoblast differentiation *in vitro (35)*. Activation of ERK signaling was also implicated in the

21 mechanism of a rare form of OI due to loss-of-function variants in *CCDC134 (36)*. These

22 seemingly conflicting effects suggest a cell and stage-specific action of this pathway, and likely a

23 crosstalk with other signaling events during osteoblast differentiation (37, 38).

1   Co-activation of ERK signaling and SOX9 expression has been reported in differentiating

2 osteoblasts (39) and in developing cartilage (40), and they are both important regulators of

3 skeletal development throughout osteochondral differentiation. SOX9 is regulated by the

4 ERK/MAPK signaling pathway (39, 41, 42). We observed altered spatio-temporal expression of

5 *Sox9* and increased SOX9 protein level in our mouse models. Moreover, genetic deletion of *Sox9*

6 in cells expressing mutant IFITM5 led to improvement in the growth plate architecture and

7 improved the low bone mass phenotype (**Fig. 8**), supporting that SOX9 plays a critical role in the

8 pathological mechanism of OI type V. SOX9 is a master transcription factor in chondrocyte

9 differentiation (43, 44), and is downregulated in hypertrophic chondrocytes. Persistent

10 expression of *Sox9* in the hypertrophic zone disrupts terminal chondrocyte maturation and

11 endochondral bone formation (45-47). Interestingly, impaired chondrocyte hypertrophy, as seen

12 in *Rosa26^{mIfitm5}*; Prx1-Cre mutant mice (**Fig. 3C, D**), has been reported in mouse models that

13 have constitutively activated FGFR3 and MAPK signaling (48-52). In mice expressing the

14 thanatophoric dysplasia type II activating *FGFR3* mutation, the defect in chondrocyte maturation

15 and bone formation was linked to increased SOX9 protein stability (51, 52). Moreover, *Sox9* has

16 been shown to down regulate *Runx2* (53), or inhibit its activity (54), during both chondrocyte

17 hypertrophy and endochondral ossification. In humans, campomelic dysplasia caused by *SOX9*

18 haploinsufficiency is associated with chondrocyte hypertrophy and increased RUNX2 level (44,

19 54). Hence, gain of SOX9 function can affect not only chondrogenesis, but also bone formation

20 derived from chondrogenic cells in the growth plate.

21   Conditional expression of the mutant *Ifitm5* in the *Rosa26^{mIfitm5}*;Prx1-Cre and

22 *Rosa26^{mIfitm5};Acan-Cre ERT2* mice resulted in low bone mass phenotype, as seen in individuals

23 with OI type V. Biomechanical testing in the *Rosa26^{mIfitm5};Acan-Cre ERT2* model demonstrated

1   reduced ductility and increased bone stiffness, correlating with the findings in other OI mouse

2   models (55, 56). Although not associated with rhizomelic short stature, OI type V can present

3   with variable longitudinal growth restriction (9, 10), and clinical observations have led others to

4   suggest a defect in growth plate development and function (10, 57). Our mutant mice exhibit

5   cartilage overgrowth at the knees and ankles that progresses to joint contractures (**Fig. 5**).

6   Interestingly, severe joint contractures and ankylosis have been reported in some individuals

7   with OI type V (58). In a small cohort of patients, we discovered milder joint dysfunction, most

8   frequently manifested as limited range of motion at the hips and elbows (**Fig. S11, Table S1**).

9   A limitation of our model is the expression of the mutant protein from the *Rosa* locus.

10   The Prx1-Cre mouse model targets cells of the limb bud and cranial mesenchyme, while sparing

11   the axial skeleton, and thus was not suitable to model scoliosis or other spinal abnormalities.

12   Our mouse models demonstrated abnormal cartilage formation, but they did not recapitulate the

13   hypertrophic callus or calcification of interosseous membranes as seen in the human patients.

14   However, the similar tissue abnormalities with human studies both here and in the literature, the

15   findings in heterologous systems in zebrafish and cell models (MC3T3), and the rescue of both

16   cell and fish phenotypes with ERK inhibition and of the mouse phenotype by genetic deficiency

17   of *Sox9*, together support the relevance of these mechanistic findings to the human condition.

18   In summary, we present here a conditional mouse model for OI type V, expressing the

19   mutant *Ifitm5* allele under *Rosa26* promoter. Conditional expression of mutant *Ifitm5* in cells of

20   the osteo-chondroprogenitor, or chondrogenic lineages, resulted in low bone mass, growth

21   restriction, cartilage overgrowth and joint deformities, mimicking the human phenotype.

22   Importantly, we demonstrated a chondrogenesis defect that, together with a mineralization

23   defect, is likely driven by activated ERK signaling and elevated SOX9 downstream of the

1   *IFITM5* mutation. The rescue by ERK inhibition and *Sox9* deficiency points to potential

2   therapeutic approaches for this disorder and have a broader impact on the understanding of

3   mechanisms governing skeletal homeostasis.

4

5

6

7

8

9

10

11

12

13

14

15

16

17

18

19

20

21

1 **METHODS**

2 <u>Sex as a biological variable</u>: Both male and female mice were used for described experiments.

3 For zebrafish study, sex-specific differences were not considered because zebrafish sex

4 differentiation occurs at 21-23 days post fertilization, while all experiments reported here were

5 concluded by day 5 post fertilization. The human study included both male and female

6 participants.

7 *Ifitm5* conditional *Rosa26* knock-in mouse model: We generated a knock-in *Rosa26* mouse

8 model by introducing the mutant *Ifitm5* cDNA (m*Ifitm5*) into the *Rosa26* locus using previously

9 described approaches(22, 59). The murine *Ifitm5* cDNA was introduced into pCMV-Tag1 vector

10 to add an in-frame Flag tag at the c terminus, and *in vitro* mutagenesis was performed to obtain

11 the c.-14C>T mutation. The Flag-tagged mutant cDNA was then introduced to pRosa26-DEST

12 vector using Gateway recombination cloning. pRosa26-DEST was a gift from Nick Hastie &

13 Peter Hohenstein [Addgene plasmid # 21189; http://n2t.net/addgene:21189;

14 RRID:Addgene_21189 (59)]. Targeting of the construct to the *Rosa26* locus in C57BL/6N

15 mouse embryonic stem (ES) cells (JM8A3) was performed via electroporation by the Genetically

16 Engineered Rodent Model core at Baylor College of Medicine (BCM). ES cell clones were

17 screened for correct targeting by PCR amplification of the 5' region, the knocked-in Ifitm5

18 cDNA insert, and the 3' region within Rosa26 locus (**Table S2**). Correct copy number

19 (heterozygosity) of the knocked-in allele was validated by real time PCR using Neo TaqMan

20 gene dosage assay. Following initial PCR screening, selected clones were validated by southern

21 blotting, as previously described(22). Correctly targeted ES cells were then expanded and

22 assessed for morphology and karyotyping prior to generation of chimeric animals via

23 microinjection and transfer of C57BL/6NTac-A[tm1.1Arte], Tyr[tm1Arte] (Taconic model number 11227)

1   blastocysts. Sanger sequencing confirmed the insertion of knocked-in allele in founder animals.

2   Chimeras were crossed to C57BL/6NTac-A[tm1.1Arte], Tyr[tm1Arte] mice to generate N1 animals,

3   inheritance of the knock-in allele in N1 animals was confirmed by Sanger sequencing, and the

4   N1 generation was backcrossed to C57BL/6 to generate N2 mice. For all studies described, mice

5   were maintained on a C57BL/6 genetic background. Mice that are heterozygous for the *Rosa26*

6   knock-in mutant *Ifitm5* allele (*Rosa26^{mIfitm5/+}*) were crossed to Cre-recombinase expressing

7   mouse lines (*Cre/-*), to generate the following genotypes: mutant (*Rosa26^{mIfitm5/+}; Cre/- mice*)

8   and littermate controls (including *Cre/-* mice, *Rosa26^{mIfitm5/+}* mice, and *Rosa26^{+/+}* mice). The Cre

9   mouse lines that were used include the Paired related homeobox 1-Cre (Prx1-Cre) transgenic

10   line, the Osteocalcin-Cre (OC-Cre) transgenic line, the rat 2.3 kb Col1a1 transgenic line

11   Tg(Col1a1-cre)2Bek (Col1a1-Cre), and the *Agc1^{tm(IRES-CreERT2)} line (Acan-Cre* ERT2) that

12   expresses tamoxifen-inducible CreER^{T2} from the aggrecan promoter. The *Acan-Cre* ERT2

13   inducible Cre recombinase was activated by administration of Tamoxifen (10 mg/kg/dose) via

14   intraperitoneal injections, starting at P.10 and until P.15. For *Sox9^{fl}* rescue experiments,

15   *Rosa26^{mIfitm5};Acan-Cre ERT2* mice were crossed to *Sox9^{fl/fl}* mice, Cre recombinase was activated

16   as above, and the following littermates were collected for analysis: *Rosa26^{mIfitm5};Sox9^{fl/+};Acan-*

17   *Cre ERT2 and Sox9^{fl/+};Acan-Cre ERT2* (in comparison to *Rosa26^{mIfitm5};Acan-Cre ERT2*). In

18   addition, *Rosa26^{mIfitm5};Acan-Cre ERT2* mice were crossed to *Rosa26* knock-in tdTomato reporter

19   line (B6.Cg-*Gt(ROSA)26Sor^{tm9(CAG-tdTomato)Hze}*/J, here referred to as Ai9 reporter mice) to generate

20   *Rosa26^{mIfimt5/Ai9};Acan-Cre ERT2* mice.

21   Generation of IFITM5-expressing zebrafish: The expression of mutant IFITM5 in zebrafish

22   (*Danio rerio*) was achieved by injecting zebrafish embryos (*AB* strain) with mutant human

23   *IFITM5* mRNA at the one cell stage [30 minutes to 1 hour post fertilization (*hpf*)]. In brief, the

1 human wild type or mutant *IFITM5* cDNA was introduced into pCS2+ expression vector. To

2 obtain the human *IFITM5* cDNA, total mRNA was extracted from induced pluripotent stem cells

3 (iPSCs) that were generated from an individual with OI type V and differentiated into osteoblasts

4 for 14 days, using previously described methods (60, 61). Total mRNA served as a template to

5 generate cDNA (Superscript III First Strand RT-PCR kit, Invitrogen) and mutated or wild type

6 IFITM5 cDNAs were amplified (**Table S2**). Mutated and wild type *IFITM5* mRNA, or mCherry

7 mRNA, were transcribed *in vitro* from pCS2+ vector using mMessage SP6 transcription kit

8 (Invitrogen), and 100 pg were injected/embryo. At 120 *hpf*, embryos were fixed in 4%

9 paraformaldehyde and then stained in 0.1% Alcian blue solution. For ERK/MEK inhibitor rescue

10 experiments, embryos were injected with mutant *IFITM5* mRNA, then randomly allocated at 5

11 *hpf* to treatment (InSolution MEKI/II Inhibitor III, PD0325901, EMD Millipore at 0.5 uM) or

12 control (DMSO) groups. Treatment was applied daily to fresh E3 water and at 120 *hpf* embryos

13 were fixed and stained as above for morphology assessment.

14 Cell culture: All cells were cultured at 37°C and 5% CO_2 in a humid environment. MC3T3-E1 or

15 ATDC5 cells (ATCC) were cultured according to ATCC guidelines. A Tet-on system was

16 employed to stably express *Ifitm5$^{c.-14C>T}$* under Doxycyclin induction in MC3T3 cells. In brief,

17 cells were transfected with a *piggyBac*-based system to insert two transgenes into the genome:

18 *Ifitm5$^{c.-14C>T}$* (pTight-TRE- *Ifitm5$^{c.-14C>T}$*) and rtTA (Tetracycline responsive transactivator,

19 pCMV-rtTA). Transfected cells were selected with 2 μg/mL puromycin (Gibco) and 500 μg/mL

20 G418 (Gibco). Stable cells were maintained in growth media (alpha MEM with 10% fetal bovine

21 serum, 1% glutamine and 1% penicillin/streptomycin) containing Puromycin and G418. *Ifitm5$^{c.-}$*

22 *$^{14C>T}$* expression was induced by Doxycyline administration (1.2 uM; Sigma-Aldrich). For *in*

23 *vitro* osteogenic differentiation, cells were incubated for 14 days in growth media (alpha MEM

1 with 10% fetal bovine serum, 1% glutamine and 1% penicillin/streptomycin), containing beta

2 glycerophosphate (10 mM, Sigma-Aldrich), ascorbic acid (100 ug/ml, Sigma-Aldrich) and

3 BMP2 (100 ng/ml, R&D Systems). ERK inhibitor rescue was studied by applying U0126

4 (Millipore Sigma, at 5 or 10 uM) or vehicle (methanol). Alizarin red S staining was performed

5 after fixation of cells with 4% formalin. For *in vitro* chondrogenic differentiation of ATDC5,

6 cells were incubated for 21 days in growth media (DMEM/F12 with 10% fetal bovine serum, 1%

7 glutamine and 1% penicillin/streptomycin), containing ITS supplement (Insulin-Transferrin-

8 Selenium, Gibco).

9 <u>Marrow stromal cells (MSC) differentiation *in vitro*</u>: Flushed bone marrow cells from *Rosa26*

10 knock-in mutant *Ifitm5* mice ($Rosa26^{mIfitm5/+}$) were treated with 2uM TAT Cre-recombinase

11 (Excellgen, EG-1001) in low-serum growth media (alpha MEM with 1% fetal bovine serum, 1%

12 glutamine and 1% penicillin/streptomycin) to activate the Ifitm5 mutation. For osteoblast

13 differentiation, MSC were plated at $8x10^5$/ml into 12-well plate, incubated with Cre-recombinase

14 overnight, and allowed to recover for 24 hours in serum-rich growth media (20% fetal bovine

15 serum). Osteogenic differentiation media (alpha MEM with 10% fetal bovine serum, 1%

16 glutamine, 1% penicillin/streptomycin, 10 mM beta glycerophosphate and 100 ug/ml ascorbic

17 acid) was applied to confluent cultures and changed every other day for a total of 7 days before

18 RNA was extracted for qPCR analysis. For chondrogenic differentiation, MSC were pre-treated

19 with Cre-recombinase, then plated at $1.5x10^6$/ml (150,000 cells/well) into v-shaped 96-well

20 plates and span-down (500g, 5 min) to pellet culture. Chondrogenic media

21 (StemXVivo® Chondrogenic Media and Chondrogenic Supplement, R&D Systems) was

22 refreshed every 3 days for a total of 21 days. Cells were fixed in 4% glutaraldehyde and stained

1   with Alcian Blue. Condensed cartilaginous structures were embedded in OCT media (Tissue-

2   Tek® O.C.T. Compound, Sakura), and cryo-sectioned at 7 um for staining.

3   <u>Isolation and flow cytometry analysis of periosteal and bone marrow skeletal progenitor cells</u>: To

4   isolate periosteal cells, dissected femurs and tibia were placed in PBS and the overlaying muscle

5   were carefully removed. Bones were then incubated in ice-cold 1% FBS for 15 minutes, and the

6   loosely associated periosteum was scraped off using forceps. The periosteal tissues were

7   incubated with 0.2% collagenase and 10% FBS in PBS at 37°C for one hour. The dissociated

8   periosteal cells were washed in PBS, filtered with a 40-μm cell strainer, and resuspended at

9   ~1×10^7 cells/mL. To isolate bone marrow cells, femurs and tibia cleaned of periosteum were

10   crushed in 1% FBS using a mortar and pestle. The remaining bone was further fragmented using

11   dissection scissors. The bone fragments in 1% FBS were washed then incubated in 0.2%

12   collagenase and 10% FBS in PBS at 37°C for one hour, as previously described(62). After

13   incubation the dissociated cells were washed in PBS, filtered through a 40-μm cell strainer, and

14   resuspended at ~1×10^7 cells/mL. To analyze skeletal stem/progenitor cell population, cells were

15   stained with CD45-pacific blue (clone:30-F11), CD31-eFluor 450 (clone:390), and Ter119-

16   BV605 (clone: Ter119) in combination with CD140a-APC (clone: APA5) and CD105-PE-Cy7

17   (clone: MJ7/18). Antibodies were purchased from eBioscience. DAPI was used for viable cell

18   gating. Flow cytometric experiments were performed in the BCM Cytometry and Cell Sorting

19   Core using an LSR Fortessa (BD bioscences, San Jose, CA). Data were analyzed with FlowJo

20   Software (TreeStar, Ashland, OR) and represented as dot plots of fluorescence intensity.

21   <u>RNA extraction, real-time qPCR and RNA sequencing</u>: Bone tissues (femur or tibia) were

22   collected from 2 months old *Rosa26^mIfitm5/+;*Prx1-Cre, *Rosa26^mIfitm5/+;*OC-Cre and

23   *Rosa26^mIfitm5/+;*Col1a1-Cre mice. Cartilage tissue (rib cage) was collected from

1   *Rosa26^{mIfitm5/+};Acan-Cre* ERT2 mice at P.6 that were activated by Tamoxifen subcutaneous

2   injection (10 mg/kg/dose) at P.3-P5. Total RNA was extracted in Trizol reagent (Ambion) using

3   TissueLyser (Qiagen). The iScript cDNA synthesis kit (Bio-Rad) or SuperScript III (Invitrogen)

4   were used to synthesize cDNA according to the manufacturer's protocol. Real-time qPCR was

5   performed on LightCycler instrument (Roche) using FastStart Essential DNA Master reagent

6   (Roche) with *GAPDH* or *B2m* (beta-2 microglubulin) as internal control. For RNA sequencing,

7   femurs were collected from 5 weeks old *Rosa26^{mIfitm5/+};Acan-Cre* ERT2 mice that were activated

8   by Tamoxifen intraperitoneal injection (10 mg/kg/dose) at P.10. Total RNA from pulverized

9   bone was extracted using Trizol reagent (Ambion) and further purified by phenol-chloroform

10   precipitation. Total RNA (1 ug) was subjected to rRNA-depletion based library preparation and

11   sequencing (Azenta Life Sciences). Between 25.5 and 34 million paired-end reads were

12   generated for each sample. The alignment was performed using STAR aligner with mm39 as the

13   reference genome. Normalization, differential expression, hierarchical clustering, and GO

14   analysis were then performed using RNA-Seq analysis pipeline in Partek Genomics Suite

15   (Partek). Differential gene analysis was performed using DESeq2 and statistical significance was

16   determined by 2-way ANOVA, which is built into the Partek Genomics Suite RNA-Seq analysis

17   pipeline. The significantly differential expressed genes (fold change >2 and false discovery rate

18   < 0.05) were then used for GO Analysis. Chondrogenic and osteogenic genes were selected for

19   heatmap generation based on previous report (63). <u>Protein extraction, Reverse Phase Protein</u>

20   <u>Array (RPPA), and western blot</u>: Protein was extracted from calvaria of transgenic *Ifitm5^{c.-14C>T}*

21   mice(19) in modified Tissue Protein Extraction Reagent (ThermoFisher Scientific) containing

22   protease and phosphatase inhibitors cocktail (Roche), using TissueLyser (Qiagen). The protein

23   concentration was measured using a BCA kit (ThermoFisher Scientific) and the lysate was

1   diluted to 0.5 mg/ml in RPPA lysis buffer containing SDS sample buffer and 0.25% β-

2   mercaptoethanol. The RPPA was conducted by the Antibody-based Proteomics Core at BCM

3   using a standardized protocol (64). In total, 8 mutant transgenic (*Ifitm5$^{c.-14C>T}$*), 8 wild type

4   transgenic and 8 non-transgenic littermates bone samples were included in the experiment. Each

5   sample was assayed in 3 technical replicates to account for technical variation. For western blot

6   analysis, 25-50 ug of total protein was loaded on 4-15% SDS-PAGE gradient gel (Bio-Rad) and

7   transferred to PVDF membrane (Millipore Sigma). Membrane was blocked in 5% skim milk and

8   incubated overnight at 4°C with primary antibody: anti-Phospho-p44/42 MAPK (Erk1/2)

9   Thr202/Tyr204 (Cell Signaling, 9101S), p44/42 MAPK (Erk1/2) (Cell Signaling, 4695S), anti-

10   SOX9 (EMD Millipore AB5535), anti-IFITM5 (Abcam, ab230863), anti-alpha Tubulin

11   (Millipore Sigma, T5168) and anti-GAPDH (Millipore Sigma, G9295). Signal was captured by

12   film or via ChemiDoc imager (Bio Rad).

13   <u>Histology and Immunohistochemistry (IHC)</u>: Bone samples from OI type V patient and

14   unaffected control were obtained when subjects were undergoing skeletal surgery for a medical

15   indication. The fragments of bone removed during surgery, which otherwise would have been

16   discarded, were collected, and processed for histology. Mouse hindlimbs were collected at age 2

17   weeks and 2 months. Tissues were fixed in 4% paraformaldehyde (PFA) overnight at 4°C and

18   stored in 70% ethanol. Paraffin-embedded tissues were sagittally sectioned at 7µm. Hematoxylin

19   and Eosin staining, Alcian Blue and Nuclear Fast Red staining, were performed according to

20   standard methods. Toluidine Blue staining was performed using manufacturer's orders

21   (VitroView). For IHC, samples were deparaffinized, re-fixed in 4% PFA for 30 minutes, and

22   incubated at 60°C in Target Retrieval Solution, pH 6.1 (Dako) for antigen retrieval. Samples

23   were treated in 3% hydrogen peroxide for 30 minutes at room temperature, followed by blocking

1   with 5% normal goat serum. The following primary antibodies were applied overnight at 4°C:

2   anti-COL10A1 (DSHB, Iowa City, IA, USA X-AC9), anti-SOX9 (EMD Millipore AB5535), or

3   anti- Phospho-p44/42 MAPK (Erk1/2) Thr202/Tyr204 (Cell Signaling, 9101S). Anti-rabbit

4   secondary antibody (Vectastain ABC system, Vector Laboratories) was applied, and DAB

5   (Vector SK-4100) staining performed per manufacturer instruction. Slides were stained with

6   Hematoxylin and mounted using Cytoseal XYL xylene-based mounting medium (Thermo

7   Scientific). Images were taken with a light microscope (Axioplan 2, Zeiss), or using Zeiss

8   AxioScan_Z1 whole slide scanner by the BCM RNA In-Situ Hybridization core.

9   Skeletal radiographs: Radiographic images of $Rosa26^{mIfitm5/+}$; Cre/- mice were taken with the

10 Kubtec XPERT80 (Kubtec X-ray).

11 Skeletal preparations: P.21 $Rosa26^{mIfitm5/+}$; Cre/- mice mutant mice and littermate controls were

12 sacrificed and fixed with 95% Ethanol, then stained overnight in Alcian blue (containing 0.015%

13 Alcian blue 8GX, 20% Acetic acid, and 80% Ethanol 95%), and soaked in 2% KOH solution for

14 24 hours to remove remnants of soft tissue. Skeletal preps were then stained overnight in

15 Alizarin red solution (containing 0.005% Alizarin red S in 1% KOH), cleared in 1% KOH/20%

16 glycerol solution, and stored in glycerol/95% Ethanol 1:1 solution.

17 Immunofluorescence imaging: Bones were collected from 5 weeks old $Rosa26^{mIfimt5/Ai9}$; $Acan-Cre$

18 $ERT2$ mice, fixed in 4% paraformaldehyde and decalcified in 10% ETDA. Samples were

19 embedded in OCT media (Tissue-Tek® O.C.T. Compound, Sakura), cryo-sectioned at 10 um and

20 mounted to adhesive microscope slides using Tape-Transfer system (Leica). Slides were

21 counterstained with DAPI (IHC World) and sealed using ProLong™ Glass Antifade mounting

22 media (Invitrogen) according to the manufacturer's instructions. Images were acquired with

1   Zeiss LSM 780 confocal microscope in the Optical Imaging and Vital Microscopy Core at BCM.

2   Images were processed with the ImageJ software.

3   <u>Micro-CT analysis</u>: Spines and right femurs were scanned in 70% ethanol using a Scanco μCT-

4   40 micro-CT system (Scanco Medical, 55kVp and 145μA X-ray source), and scans were

5   reconstructed at a 16μm isotropic voxel size. Trabecular bone of L4 vertebrae and the distal

6   metaphyses of right femurs were analyzed using Scanco software by manually contouring

7   trabecular bone. For vertebrae, the region of interest (ROI) was defined as the trabecular volume

8   between the L4 vertebral endplates. For femurs, trabecular ROI was defined proximal to the

9   distal femoral growth plate and the number of slides analyzed was adjusted to femoral length

10   (femur length was measured from the top of the femoral head to the bottom of the medial

11   condyle): 75 slides (=1.2 mm) were analyzed for 2 months old Prx1-Cre and OC-Cre mouse

12   models control femurs; 55-60 slides were analyzed for 5 weeks old *Acan-Cre ERT2* control

13   femurs; and 45-50 slides were analyzed for mutant femurs (across all models). Quantification of

14   trabecular parameters was performed using the Scanco software with a threshold value of 230.

15   These parameters include bone volume/total volume (BV/TV), trabecular number (Tb.N) and

16   trabecular thickness (Tb.Th), connectivity density (Conn.D) and tissue mineral density (TMD)

17   (65). Cortical bone parameters of the femoral midshaft were measured at the exact center and at

18   the distal 75% of femur length using the automated thresholding algorithm included in the

19   Scanco software. Trabeculae in contact with cortical bone were manually removed from the ROI

20   (11 slides analyzed per location, threshold 210). The cortical parameters include total cross-

21   sectional area (Tt.Ar), cortical bone area (Ct.Ar), marrow area (Ma.Ar), cortical thickness

22   (Ct.Th), cross-sectional moments of inertia (CSMI), anterior-posterior diameter, and tissue

23   mineral density (TMD) (65). Between six to eight spines and femurs were scanned per group.

1   Biomechanical measurement: Femurs were collected from 5 weeks old $Rosa26^{mIfitm5/+}$;$Acan$-Cre

2   ERT2 mice that were activated by Tamoxifen intraperitoneal injection (10 mg/kg/dose) at P.10.

3   Bones were collected, stripped of soft tissues, wrapped in saline-soaked gauze, and frozen at –

4   20°C until analyses were performed. The femurs were tested to failure in three-point bending at a

5   rate of 0.1 mm/sec and were oriented in the test fixture such that the anterior surface was in

6   compression and the posterior surface in tension. Femurs were tested wet at room temperature

7   using displacement mode with an Instron 68SC-2 microtester (Instron Inc., Norwood MA). The

8   test fixture span was 3.61mm. A 100N load cell was used to collect data, and load and

9   displacement data were captured at rate of 40Hz by using BLUEHILL Software (Instron 68SC-

10   2). The maximum load was determined by finding the highest load value recorded before the

11   specimen fractured. The region of the load-displacement curve between 1N and the maximum

12   load was separated into 5 segments and the fitted line of the segment with greatest slope was

13   defined as the stiffness. A line representing 10% degradation of this stiffness was used to define

14   the yield point. The elastic region was identified as the region from the completion of the preload

15   to the yield point. The post-yield region was identified as the region from the yield point until

16   point of specimen fracture. Using a trapezoidal numerical integration method, the work to

17   fracture was calculated as the area under the load-displacement curve. The cross-sectional

18   geometry of each bone as determined by microCT image analysis was used to convert the

19   maximum load and stiffness data into ultimate stress and elastic modulus values using beam

20   theory.

21   OI type V patient chart review: We conducted a retrospective chart review on seven individuals

22   with OI type V at three expert skeletal centers in the U.S.: Baylor College of Medicine, Houston,

23   TX, Oregon Health and Sciences University, Portland, OR, and Omaha Children's Hospital,

Omaha, NE. The following data were collected from the chart review: age, sex, molecular

diagnosis of OI type V, presence or absence of typical OI type V clinical features (hyperplastic

callus, calcification of the interosseous membrane, radial head dislocation), presence or absence

of joint pathology (decreased range of motion, joint contracture, or joint ossification in the

shoulders, elbows, wrists, hips, knees and ankles). The data were collected in a standardized

format using specific data fields from all three centers.

Statistical methods: All statistical analyses used parametric unpaired tests, including one-way

analysis of variance (ANOVA) or Student's *t*-tests. Prism GraphPad software

(https://www.graphpad.com/scientific-software/prism/) or SAS 9.4 (SAS Institute Ince., 2007,

Cary, NC) was used for the statistical analysis. *P*-values<0.05 were considered significant.

Study approval: Mice and zebrafish were housed in the Baylor College of Medicine Animal

Vivarium, and all procedures were approved by the Institutional Animal Care and Use

Committee (IACUC) at Baylor College of Medicine. Bone samples from an individual with OI

type V and unaffected individual were obtained when these individuals were undergoing skeletal

surgery for a medical indication. The fragments of bone removed during surgery, which

otherwise would have been discarded, were collected and processed under a protocol approved

by the Institutional Review Board (IRB) of Baylor College of Medicine. Informed consent was

obtained from the parents or legal guardians prior to collection of samples. For the retrospective

chart review, medical records for 6 individuals were reviewed after informed consent was

obtained from participants or their legal guardians. These 6 individuals were enrolled in an

observational natural history study of osteogenesis imperfecta being conducted by the NIH Rare

Diseases Clinical Research Network's Brittle Bone Disorders Consortium (NCT02432625). For

1   one participant, who was not enrolled in the observational study, written permission was

2   obtained to review and publish deidentified phenotypic data.

3   Data availability: All data generated or analyzed during this study are included in the manuscript

4   and supporting files. "Supporting data values" file has been provided for all numerical data.

5   RNA sequencing data were deposited to GEO database (accession number GSE268601).

6

7

8

9

10

11

12

13

14

15

16

17

18

19

20

1 **AUTHOR CONTRIBUTIONS**

2 Conceptualization: RM, BHL

3 Methodology & investigation: RM, IS, MEW, ASB, VCR, LO, YJ, CDL, DB, ECB, MMJ, YC,

4 RC, IL, MA, CL, DNM, CGA, DP, JDH

5 Data acquisition & statistical analysis: BCD, AC, BMS, MJ, SH

6 Subject recruitment and clinical phenotyping: AAT, AT, MW, EO, SCSN

7 Supervision: BHL

8 Writing – original draft: RM, BHL

9 Writing – review & editing: All authors reviewed and edited the manuscript

10

11
12
13

14

15

16

17

18

19

20

1 **ACKNOWLEDGEMENTS**

16

17

18
19
20
21
22
23
24
25

REFERENCES

1. Marini JC, et al. Osteogenesis imperfecta. *Nat Rev Dis Primers.* 2017;3:17052.

2. Marom R, et al. Osteogenesis imperfecta: an update on clinical features and therapies. *Eur J Endocrinol.* 2020;183(4):R95-r106.

3. Rossi V, et al. Osteogenesis imperfecta: advancements in genetics and treatment. *Curr Opin Pediatr.* 2019;31(6):708-15.

4. Jovanovic M, et al. Osteogenesis Imperfecta: Mechanisms and Signaling Pathways Connecting Classical and Rare OI Types. *Endocr Rev.* 2022;43(1):61-90.

5. Bardai G, et al. DNA sequence analysis in 598 individuals with a clinical diagnosis of osteogenesis imperfecta: diagnostic yield and mutation spectrum. *Osteoporos Int.* 2016;27(12):3607-13.

6. Liu Y, et al. Gene mutation spectrum and genotype-phenotype correlation in a cohort of Chinese osteogenesis imperfecta patients revealed by targeted next generation sequencing. *Osteoporos Int.* 2017;28(10):2985-95.

7. Trancozo M, et al. Osteogenesis imperfecta in Brazilian patients. *Genet Mol Biol.* 2019;42(2):344-50.

8. Glorieux FH, et al. Type V osteogenesis imperfecta: a new form of brittle bone disease. *J Bone Miner Res.* 2000;15(9):1650-8.

9. Cho TJ, et al. A single recurrent mutation in the 5'-UTR of IFITM5 causes osteogenesis imperfecta type V. *Am J Hum Genet.* 2012;91(2):343-8.

10. Rauch F, et al. Osteogenesis imperfecta type V: marked phenotypic variability despite the presence of the IFITM5 c.-14C>T mutation in all patients. *J Med Genet.* 2013;50(1):21-4.

11. Semler O, et al. A mutation in the 5'-UTR of IFITM5 creates an in-frame start codon and causes autosomal-dominant osteogenesis imperfecta type V with hyperplastic callus. *Am J Hum Genet.* 2012;91(2):349-57.

12. Shapiro JR, et al. Phenotypic variability of osteogenesis imperfecta type V caused by an IFITM5 mutation. *J Bone Miner Res.* 2013;28(7):1523-30.

13. Lazarus S, et al. The IFITM5 mutation c.-14C > T results in an elongated transcript expressed in human bone; and causes varying phenotypic severity of osteogenesis imperfecta type V. *BMC Musculoskelet Disord.* 2014;15:107.

14. Takagi M, et al. A recurrent mutation in the 5'-UTR of IFITM5 causes osteogenesis imperfecta type V. *Am J Med Genet A.* 2013;161A(8):1980-2.

15. Moffatt P, et al. Bril: a novel bone-specific modulator of mineralization. *J Bone Miner Res.* 2008;23(9):1497-508.

16. Patoine A, et al. The osteogenic cell surface marker BRIL/IFITM5 is dispensable for bone development and homeostasis in mice. *PLoS One.* 2017;12(9):e0184568.

17. Somoza RA, et al. Transcriptome-Wide Analyses of Human Neonatal Articular Cartilage and Human Mesenchymal Stem Cell-Derived Cartilage Provide a New Molecular Target for Evaluating Engineered Cartilage. *Tissue Eng Part A.* 2018;24(3-4):335-50.

18. Hanagata N. IFITM5 mutations and osteogenesis imperfecta. *J Bone Miner Metab.* 2016;34(2):123-31.

19. Lietman CD, et al. A transgenic mouse model of OI type V supports a neomorphic mechanism of the IFITM5 mutation. *J Bone Miner Res.* 2015;30(3):489-98.

20. Rauch F, et al. Crispr-Cas9 engineered osteogenesis imperfecta type V leads to severe skeletal deformities and perinatal lethality in mice. *Bone.* 2018;107:131-42.

21. Hanagata N, et al. Effect of immunosuppressants on a mouse model of osteogenesis imperfecta type V harboring a heterozygous Ifitm5 c.-14C > T mutation. *Sci Rep.* 2020;10(1):21197.

22. Carofino BL, and Justice MJ. Tissue-Specific Regulation of Oncogene Expression Using Cre-Inducible ROSA26 Knock-In Transgenic Mice. *Curr Protoc Mouse Biol.* 2015;5(2):187-204.

23. Brown S, et al. The Prrx1eGFP Mouse Labels the Periosteum During Development and a Subpopulation of Osteogenic Periosteal Cells in the Adult. *JBMR Plus.* 2023;7(2):e10707.

24. Kawanami A, et al. Mice expressing GFP and CreER in osteochondro progenitor cells in the periosteum. *Biochem Biophys Res Commun.* 2009;386(3):477-82.

25. Deveza L, et al. Comparative analysis of gene expression identifies distinct molecular signatures of bone marrow- and periosteal-skeletal stem/progenitor cells. *PLoS One.* 2018;13(1):e0190909.

26. Ono N, et al. A subset of chondrogenic cells provides early mesenchymal progenitors in growing bones. *Nat Cell Biol.* 2014;16(12):1157-67.

27. Gomez-Picos P, et al. Limb Mesoderm and Head Ectomesenchyme Both Express a Core Transcriptional Program During Chondrocyte Differentiation. *Front Cell Dev Biol.* 2022;10:876825.

28. Mizuhashi K, et al. Resting zone of the growth plate houses a unique class of skeletal stem cells. *Nature.* 2018;563(7730):254-8.

29. Hanagata N, and Li X. Osteoblast-enriched membrane protein IFITM5 regulates the association of CD9 with an FKBP11-CD81-FPRP complex and stimulates expression of interferon-induced genes. *Biochem Biophys Res Commun.* 2011;409(3):378-84.

30. Patoine A, et al. Topological mapping of BRIL reveals a type II orientation and effects of osteogenesis imperfecta mutations on its cellular destination. *J Bone Miner Res.* 2014;29(9):2004-16.

31. Artigas N, et al. Mitogen-activated protein kinase (MAPK)-regulated interactions between Osterix and Runx2 are critical for the transcriptional osteogenic program. *J Biol Chem.* 2014;289(39):27105-17.

32. Li F, et al. Pigment epithelium derived factor regulates human Sost/Sclerostin and other osteocyte gene expression via the receptor and induction of Erk/GSK-3beta/beta-catenin signaling. *Biochim Biophys Acta Mol Basis Dis.* 2018;1864(10):3449-58.

33. Matsushita T, et al. Extracellular signal-regulated kinase 1 (ERK1) and ERK2 play essential roles in osteoblast differentiation and in supporting osteoclastogenesis. *Mol Cell Biol.* 2009;29(21):5843-57.

34. Ge C, et al. Critical role of the extracellular signal-regulated kinase-MAPK pathway in osteoblast differentiation and skeletal development. *J Cell Biol.* 2007;176(5):709-18.

35. Kang H, et al. Somatic activating mutations in MAP2K1 cause melorheostosis. *Nat Commun.* 2018;9(1):1390.

36. Dubail J, et al. Homozygous Loss-of-Function Mutations in CCDC134 Are Responsible for a Severe Form of Osteogenesis Imperfecta. *J Bone Miner Res.* 2020;35(8):1470-80.

37. Schindeler A, and Little DG. Ras-MAPK signaling in osteogenic differentiation: friend or foe? *J Bone Miner Res.* 2006;21(9):1331-8.

38. Kim JM, et al. Biphasic regulation of osteoblast development via the ERK MAPK-mTOR pathway. *Elife.* 2022;11.

39. Song JH, et al. Signaling responses of osteoblast cells to hydroxyapatite: the activation of ERK and SOX9. *J Bone Miner Metab.* 2008;26(2):138-42.

40. Yoshida T, et al. Incoherent Feedforward Regulation via Sox9 and ERK Underpins Mouse Tracheal Cartilage Development. *Front Cell Dev Biol.* 2020;8:585640.

41. Murakami S, et al. Up-regulation of the chondrogenic Sox9 gene by fibroblast growth factors is mediated by the mitogen-activated protein kinase pathway. *Proc Natl Acad Sci U S A.* 2000;97(3):1113-8.

42. Ma N, et al. The regulatory mechanism of p38/MAPK in the chondrogenic differentiation from bone marrow mesenchymal stem cells. *J Orthop Surg Res.* 2019;14(1):434.

43. Lefebvre V. Roles and regulation of SOX transcription factors in skeletogenesis. *Curr Top Dev Biol.* 2019;133:171-93.

44. Haseeb A, et al. SOX9 keeps growth plates and articular cartilage healthy by inhibiting chondrocyte dedifferentiation/osteoblastic redifferentiation. *Proc Natl Acad Sci U S A.* 2021;118(8).

45. Kim Y, et al. Generation of transgenic mice for conditional overexpression of Sox9. *J Bone Miner Metab.* 2011;29(1):123-9.

46. Hattori T, et al. SOX9 is a major negative regulator of cartilage vascularization, bone marrow formation and endochondral ossification. *Development.* 2010;137(6):901-11.

47. Lui JC, et al. Persistent Sox9 expression in hypertrophic chondrocytes suppresses transdifferentiation into osteoblasts. *Bone.* 2019;125:169-77.

48. Ali TM, et al. The recurrent homozygous translation start site variant in CCDC134 in an individual with severe osteogenesis imperfecta of non-Morrocan ancestry. *Am J Med Genet A.* 2022;188(5):1545-9.

49. Lee YC, et al. Knock-in human FGFR3 achondroplasia mutation as a mouse model for human skeletal dysplasia. *Sci Rep.* 2017;7:43220.

50. Murakami S, et al. Constitutive activation of MEK1 in chondrocytes causes Stat1-independent achondroplasia-like dwarfism and rescues the Fgfr3-deficient mouse phenotype. *Genes Dev.* 2004;18(3):290-305.

51. Shung CY, et al. Disruption of a Sox9-beta-catenin circuit by mutant Fgfr3 in thanatophoric dysplasia type II. *Hum Mol Genet.* 2012;21(21):4628-44.

52. Zhou ZQ, et al. Mutant activated FGFR3 impairs endochondral bone growth by preventing SOX9 downregulation in differentiating chondrocytes. *Hum Mol Genet.* 2015;24(6):1764-73.

53. Dy P, et al. Sox9 directs hypertrophic maturation and blocks osteoblast differentiation of growth plate chondrocytes. *Dev Cell.* 2012;22(3):597-609.

54. Zhou G, et al. Dominance of SOX9 function over RUNX2 during skeletogenesis. *Proc Natl Acad Sci U S A.* 2006;103(50):19004-9.

55. Claeys L, et al. Exploration of the skeletal phenotype of the Col1a1 (+/Mov13) mouse model for haploinsufficient osteogenesis imperfecta type 1. *Front Endocrinol (Lausanne).* 2023;14:1145125.

56. Bi X, et al. Correlations Between Bone Mechanical Properties and Bone Composition Parameters in Mouse Models of Dominant and Recessive Osteogenesis Imperfecta and the Response to Anti-TGF-beta Treatment. *J Bone Miner Res.* 2017;32(2):347-59.

57. Arundel P, et al. Evolution of the radiographic appearance of the metaphyses over the first year of life in type V osteogenesis imperfecta: clues to pathogenesis. *J Bone Miner Res.* 2011;26(4):894-8.

58. Whyte MP, et al. Coalescing expansile skeletal disease: Delineation of an extraordinary osteopathy involving the IFITM5 mutation of osteogenesis imperfecta type V. *Bone.* 2021;145:115835.

59. Hohenstein P, et al. High-efficiency Rosa26 knock-in vector construction for Cre-regulated overexpression and RNAi. *Pathogenetics.* 2008;1(1):3.

60. Jin Z, et al. Nitric oxide modulates bone anabolism through regulation of osteoblast glycolysis and differentiation. *J Clin Invest.* 2021;131(5).

61. Kho J, et al. Argininosuccinate Lyase Deficiency Causes an Endothelial-Dependent Form of Hypertension. *Am J Hum Genet.* 2018;103(2):276-87.

62. Worthley DL, et al. Gremlin 1 identifies a skeletal stem cell with bone, cartilage, and reticular stromal potential. *Cell.* 2015;160(1-2):269-84.

63. Liu CF, and Lefebvre V. The transcription factors SOX9 and SOX5/SOX6 cooperate genome-wide through super-enhancers to drive chondrogenesis. *Nucleic Acids Res.* 2015;43(17):8183-203.

64. Bu W, et al. Mammary Precancerous Stem and Non-Stem Cells Evolve into Cancers of Distinct Subtypes. *Cancer Res.* 2019;79(1):61-71.

65. Bouxsein ML, et al. Guidelines for assessment of bone microstructure in rodents using micro-computed tomography. *J Bone Miner Res.* 2010;25(7):1468-86.

Figure 1A-B
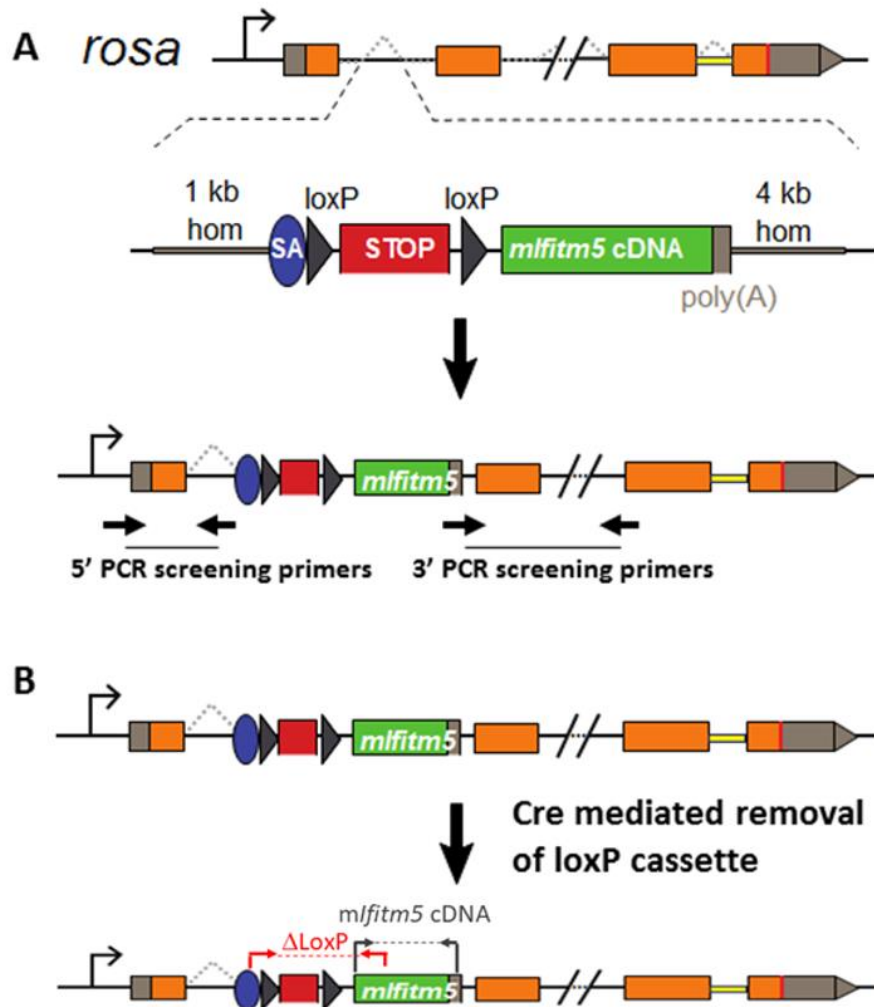
Fig. 1: Conditional *Rosa26* knock-in m*Ifitm5* mouse model. The mutant mouse *Ifitm5* cDNA was cloned into the *Rosa26*-DEST vector downstream of a loxP-polyA-loxP stop cassette. Schematic representation also indicates the approximate location of PCR screening primers (in ES cells, A) and genotyping primers (in mice, B).
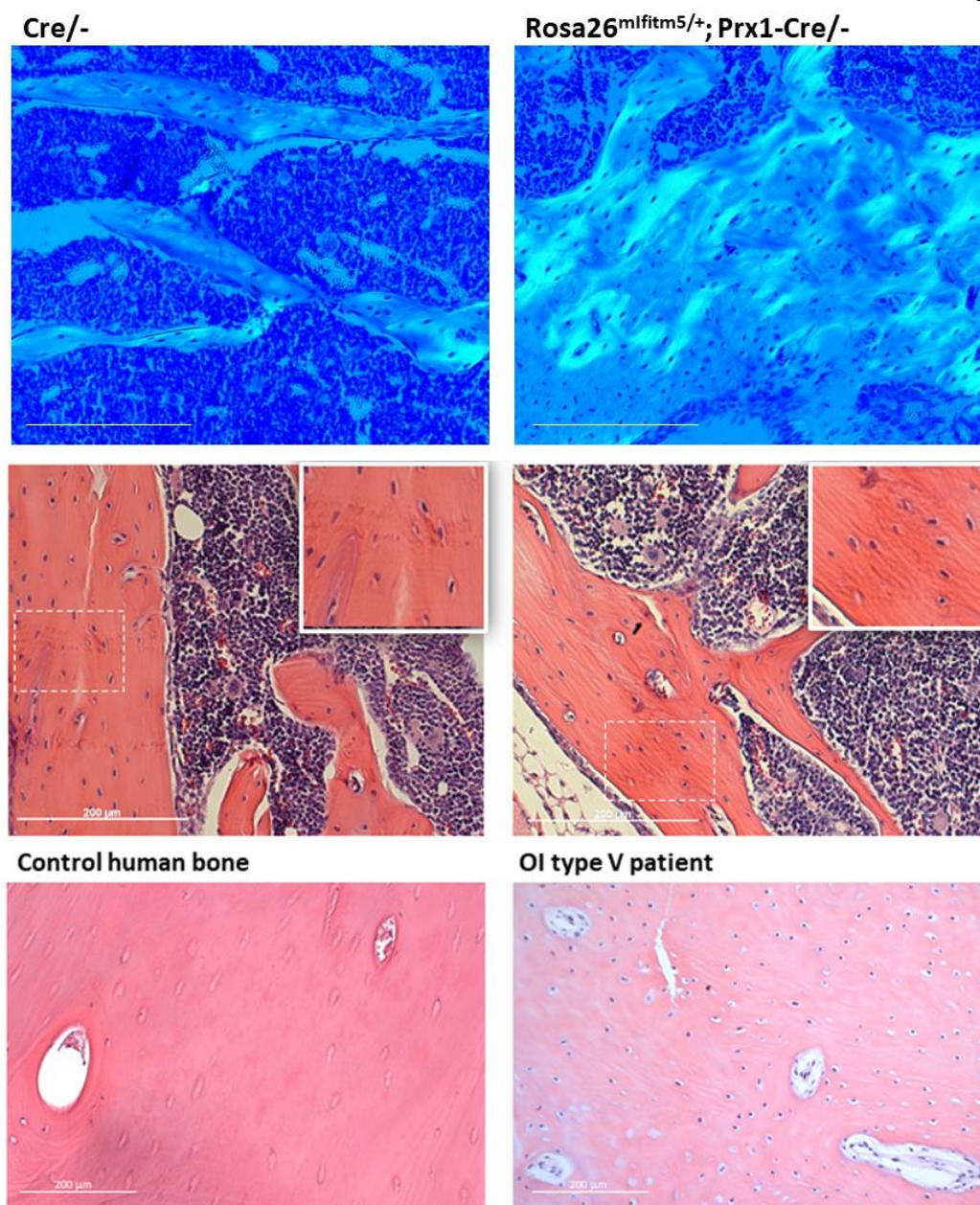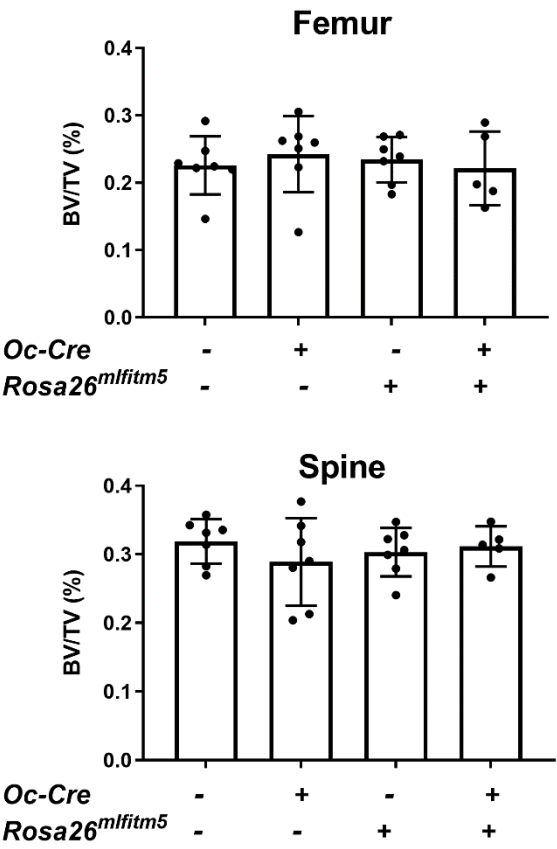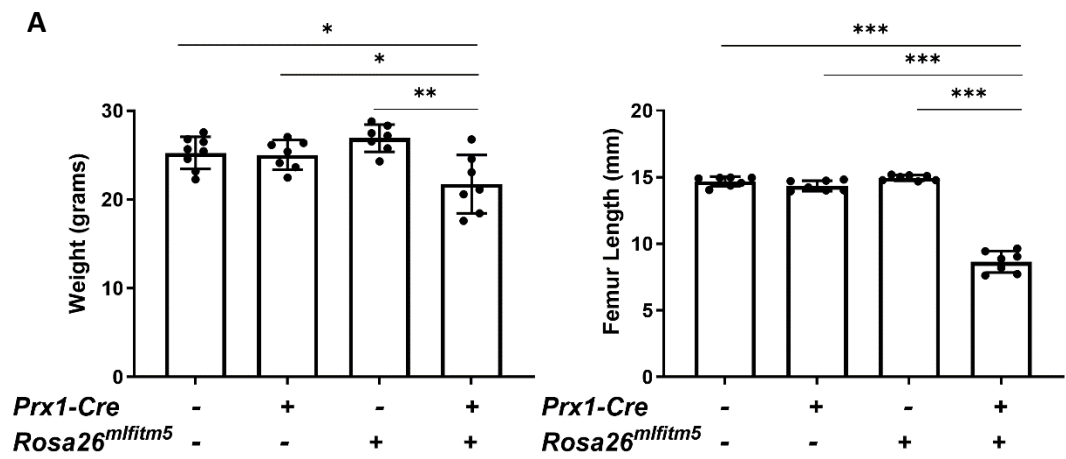
1   **Figure 2A**

2

3
4
5
6
7
8
9
10
11
12
13

1   **Figure 2B**

Cre/-

Rosa26^{mIfitm5/+}; Prx1-Cre/-

Control human bone

OI type V patient
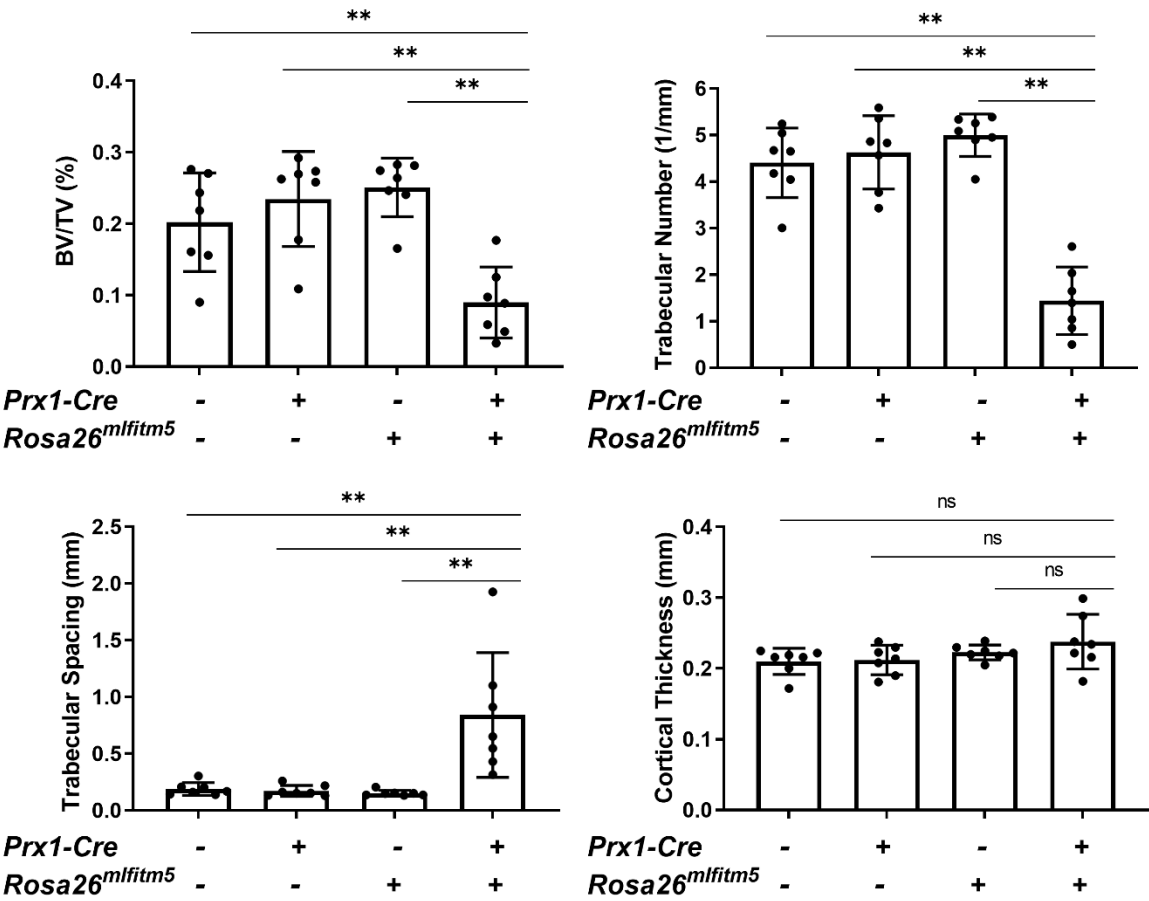
1   **Figure 2C**

1 **Fig. 2: Conditional expression of the mutant *Ifitm5* allele results in low bone mass in**

2 ***Rosa26^{mIfitm5/+}*;Prx1-Cre mice.** (A) Micro CT analysis in femurs showed significant decrease in

3 bone architectural parameters in *Rosa26^{mIfitm5/+}*;Prx1-Cre/- mutants, including the bone

4 volume/total volume (BV/TV), and trabecular number. Consistently, trabecular spacing was

5 increased. Cortical thickness was not significantly altered. Analysis preformed in 2 months old

6 males (One-way ANOVA with Tukey's post-hoc tests, n=7 per group, all comparisons to mutant

7 group. **p<0.001). (B) Histological sections show immature mesh-like bone matrix in

8 *Rosa26^{mIfitm5/+}*;Prx1-Cre/- mice, as seen in individuals with OI type V. Toluidine blue and

9 Hematoxylin & Eosin staining in *Rosa26^{mIfitm5/+}*;Prx1-Cre/- mice and littermate control (upper

10 and middle panel). Bottom panel showing human OI type V bone section for comparison. Scale

11 bar=200 um. (C) Micro CT analysis of femur and spine BV/TV showing no significant

12 difference in *Rosa26^{mIfitm5/+}*;Oc-Cre/- mice. Analysis preformed in 2 months old males (One-way

13 ANOVA with Tukey's post-hoc tests resulted not significant, n=5-7 per group, all comparisons
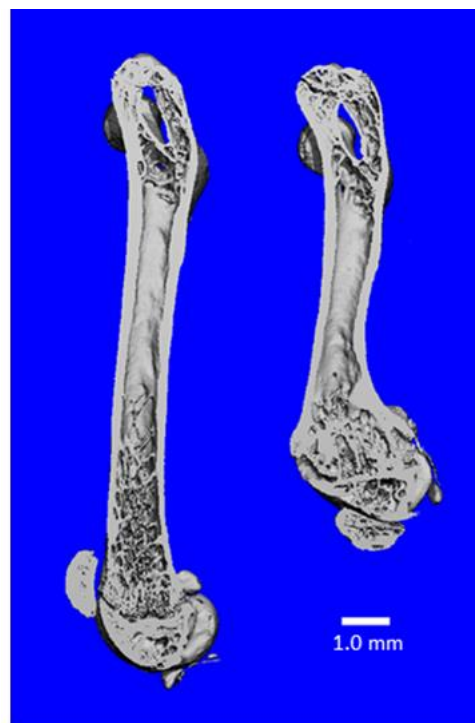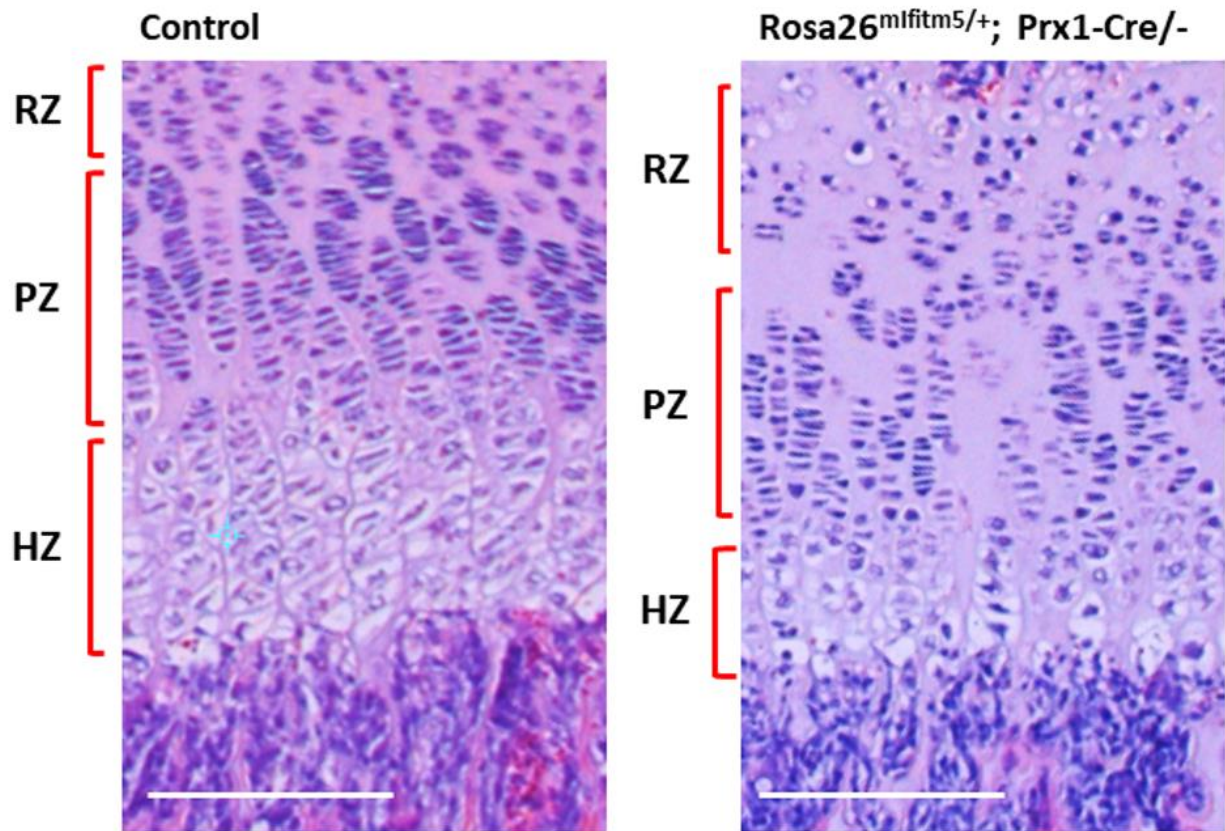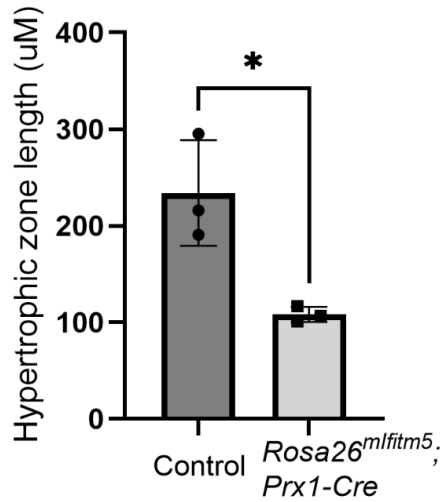
14 to mutant group).

15
16
17
18
19
20
21
22
23
24
25
26
27
28
29
30
31
32

1   **Figure 3A-B**

2

3

A

Prx1-Cre	-	+	-	+
Rosa26^{mIfitm5}	-	-	+	+

16

17

18

B

21   **Rosa26^{mIfitm5/+};**

22   **Control Prx1-Cre/-**

23

24

25

26

27

28

29

30

31

32

33

34

35

36

37

1.0 mm

1   **Figure 3C**

2
3
4
5
6
7
8
9
10
11
12
13
14

1 **Figure 3D**

2

3

4

5

6

7

8

9

10

11
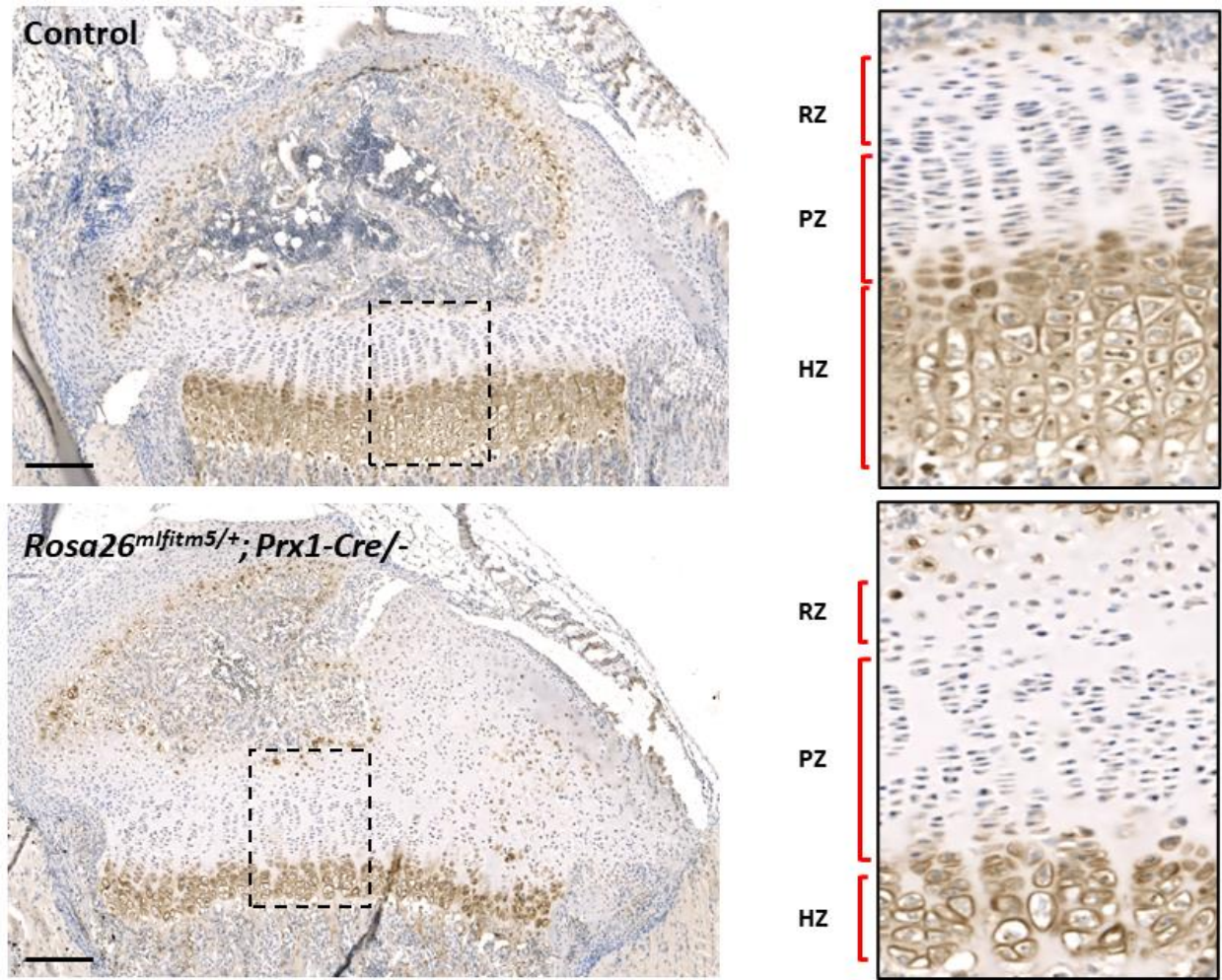
1 **Fig. 3: Conditional expression of the mutant *Ifitm5* allele results in growth restriction and**

2 **abnormal growth plate architecture in *Rosa26^{mIfitm5/+}*;Prx1-Cre mice.** (A) The body weight

3 and femur length are reduced by 10-15% and 40-50%, respectively in *Rosa26^{mIfitm5/+}*;Prx1-Cre/-

4 mutants (a summary of measurements in 2 months old male, one-way ANOVA with Tukey's

5 post-hoc tests, n=7 per group, all comparisons to mutant group. $*p< 0.05$, $**p<0.005$,

6 $***p<0.0001$). (B) A representative micro CT image of control (left) and mutant (right) femur.

7 (C) Representative histology images of proximal tibia of control (left panel) and mutant

8 (*Rosa26^{mIfitm5/+}*;Prx1-Cre/-, right panel) mice at age 2 weeks, Hematoxylin & Eosin staining,

9 showing that staggering of the proliferating chondrocyte is disrupted, and the hypertrophic zone

10 is shorter in the mutant mice. (D) Immunohistochemistry for type X collagen highlights the

11 reduced hypertrophic zone in mutant mice (*Rosa26^{mIfitm5/+}*;Prx1-Cre/-, bottom) at age 2 weeks

12 (right panel: insert magnified), and a summary of hypertrophic zone length measurements (t-test,

13 n=3 per group, $*p=0.016$). RZ= resting zone, PZ= proliferative zone, HZ= hypertrophic zone.
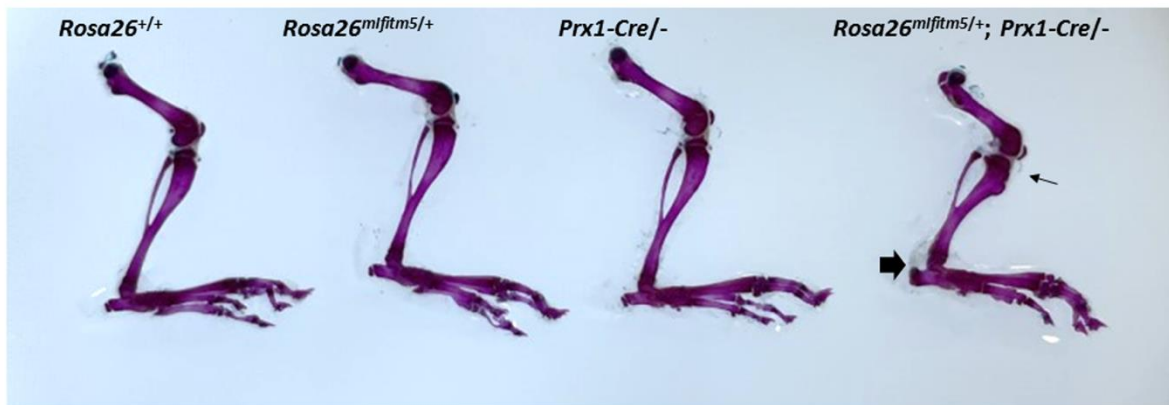
14 Scale bar = 200 um.

15

16

17

18

19

20

21

22

23

1   **Figure 4A-B**

2

3

4

5

6

7

8

9
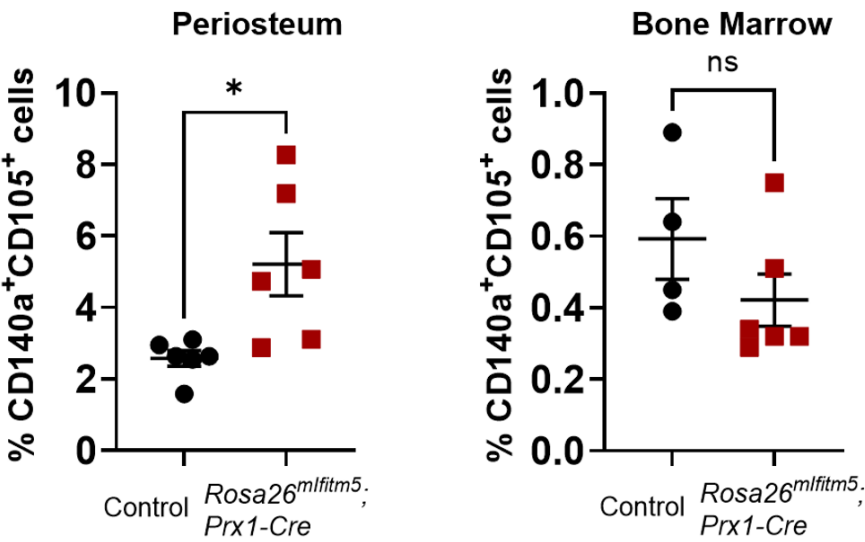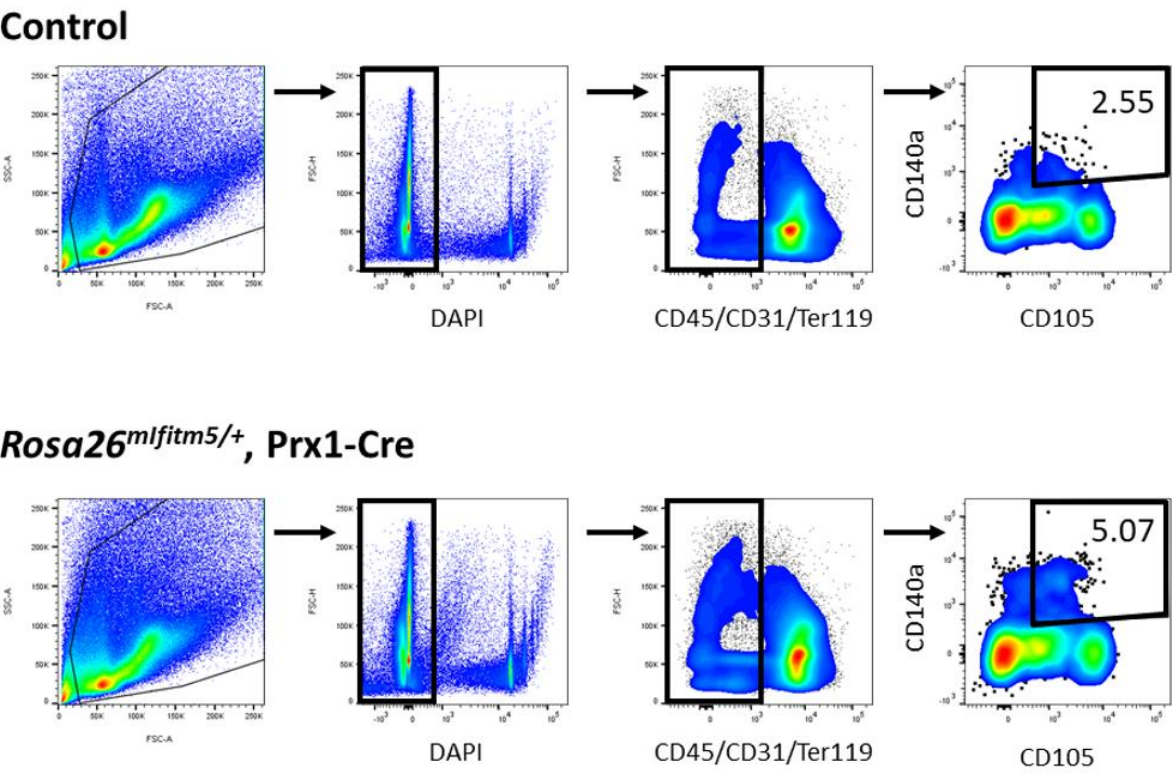
1   **Fig. 4: Conditional expression of the mutant *Ifitm5* allele results in increased periosteal**

2   **skeletal progenitors population in *Rosa26$^{mIfitm5/+}$;*Prx1-Cre mice.** (A) Flow cytometry

3   analysis of skeletal progenitor markers in cells isolated from the periosteum. (B) A significant

4   increase in CD105$^+$CD140a$^+$ population in *Rosa26^{mIfitm5}*;Prx1-Cre mutant mice was shown in the

5   periosteum, but not in the bone marrow (t-test, n=6 per group for periosteal cells, *p=0.015; n=4-

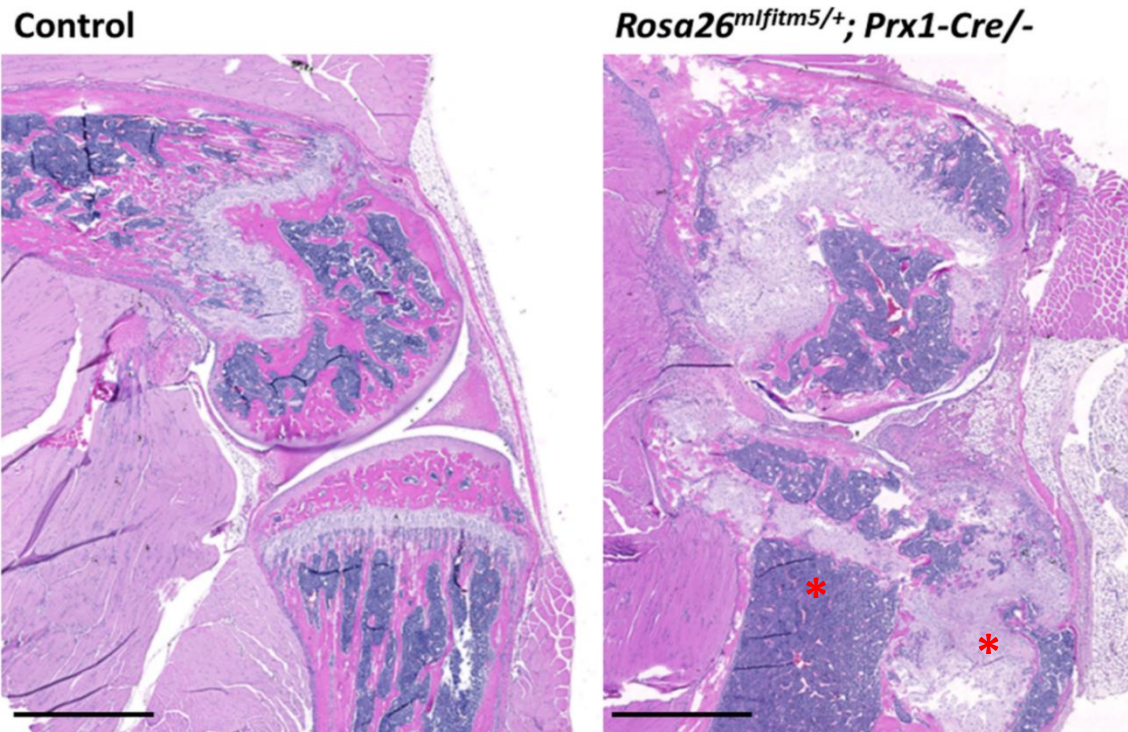6   6 per group for bone marrow cells, ns=not significant).

7

8

9

10

11

12

13

14

15

16

17

18

19

20

21

22

23

1 **Figure 5A-B**

2

3
4

5
6
7

1   **Figure 5C**

2
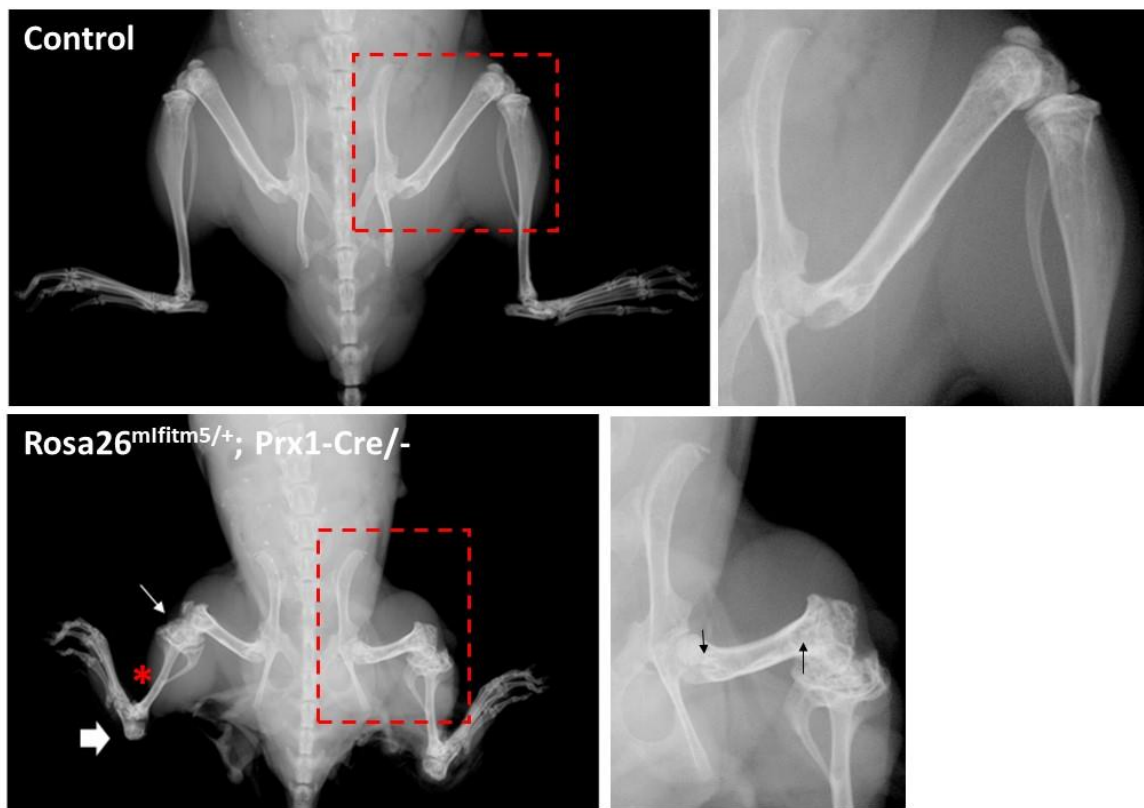
Control   *Rosa26*^{mIfitm5/+}; Prx1-Cre/-
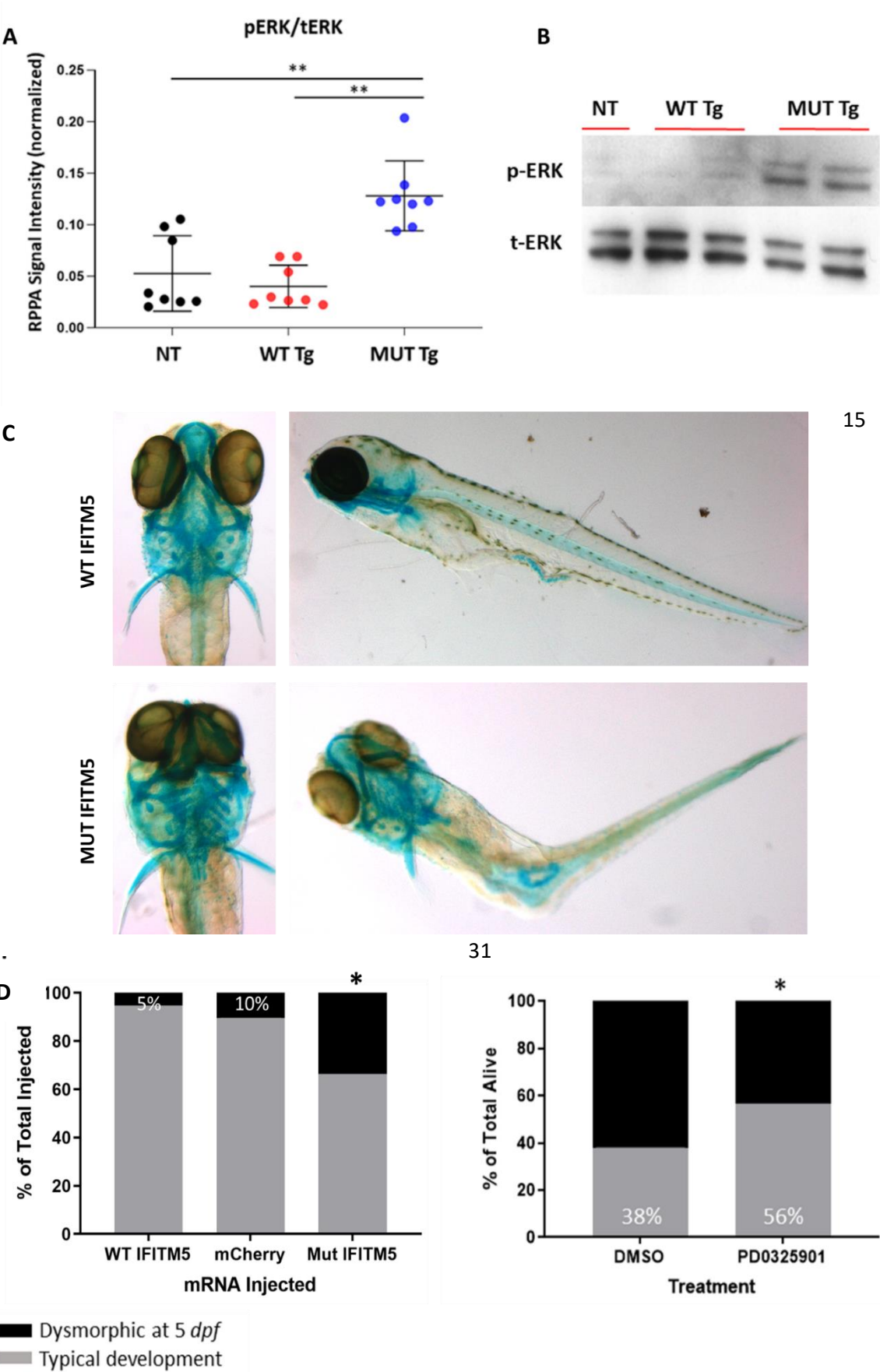
13   **Fig. 5: Conditional expression of the mutant *Ifitm5* allele in *Rosa26*$^{mIfitm5/+}$;Prx1-Cre mice**

14   **leads to progressive cartilage overgrowth and abnormal development of the ossification**

15   **centers.** (A) Skeletal preparations of 3-week-old *Rosa26*$^{mIfitm5/+}$;Prx1-Cre/- mutant and littermate

16   controls, showing skeletal deformities including shortening and bowing of the femur and tibia,

17   and partially mineralized cartilage overgrowth at the knee and ankle (thin and thick black arrows,

18   respectively). (B) Skeletal radiographs at age 2 months demonstrating short and gracile long

19   bones (red asterisk) with ossification around the knee and ankle (thin and thick white arrows,

20   respectively). Magnified inserts on the right demonstrate sclerotic lines at the femur metaphysis

21   (black arrows). (C) Representative histology images of proximal tibia of control (left panel) and

22   mutant (*Rosa26*$^{mIfitm5/+}$;Prx1-Cre/-, right panel) mice at age 2 months, showing cartilage

23   overgrowth and disruption of the endochondral ossification (red asterisk). Staining with

24   Hematoxylin & Eosin. Scale bar = 2 mm.

1 **Figure 6A-D**

2

A

pERK/tERK

** **

RPPA Signal Intensity (normalized)

0.25

0.20

0.15

0.10

0.05

0.00

NT   WT Tg   MUT Tg

B

NT   WT Tg   MUT Tg

p-ERK

t-ERK

15

C

17
18
19
20
21
22
23
24
25
26
27
28
29
30

WT IFITM5

MUT IFITM5

31

D

% of Total Injected

100
80
60
40
20
0

5%   10%

*

WT IFITM5   mCherry   Mut IFITM5

mRNA Injected

% of Total Alive

100
80
60
40
20
0

*

38%   56%

DMSO   PD0325901

Treatment

■ Dysmorphic at 5 *dpf*
▨ Typical development

1 **Fig. 6: Activation of ERK signaling contributes to the abnormal skeletal development in OI**

2 **type V.** (A) RPPA in transgenic *Ifitm5*$^{c.-14C>T}$ mouse model. Ratio of phosphorylated ERK to

3 total ERK RPPA signal intensity is increased in calvaria protein extract from mice

4 overexpressing mutant *Ifitm5* (MUT Tg), as compared to mice overexpressing wild type Ifitm5

5 (WT Tg), and non-transgenic (NT) littermates (n=8 per group, one-way ANOVA with Tukey's

6 post-hoc tests, all comparisons to Mut Tg group, **p<0.001). (B) Western blot of representative

7 RPPA samples for phosphorylated ERK (p-ERK) and total ERK (t-ERK) in transgenic *Ifitm5*$^{c.-}$

8 $^{14C>T}$ mouse model. (C) A representative image showing abnormal morphology (abnormal

9 craniofacial development and tail kinking) of embryos injected with mutant *IFITM5* mRNA

10 (MUT IFITM5, lower panel) at 5 days post fertilization, compared to normal development of

11 control zebrafish larvae (WT IFITM5, upper panel). Surviving larvae were fixed at 5 days post

12 fertilization and stained with Alcian Blue. (D) Left panel: The proportion of IFITM5 mutant

13 zebrafish that demonstrated dysmorphology (34%) was significantly greater compared to WT

14 and mCherry controls (5-10%, chi-squared test, n=113-116 per group, *p<0.001); Right panel:

15 Treatment with the ERK inhibitor PD325901 (0.2 uM) partially rescued the abnormal

16 development in IFITM5 mutant zebrafish. The proportion of IFITM5 mutant zebrafish with

17 typical development increased by 18% at 5 *dpf* (chi-squared test, n=97 in treatment group and 87

18 in vehicle group, *p<0.05).

19
20
21
22
23
24
25
26
27

1 **Figure 7A-C**
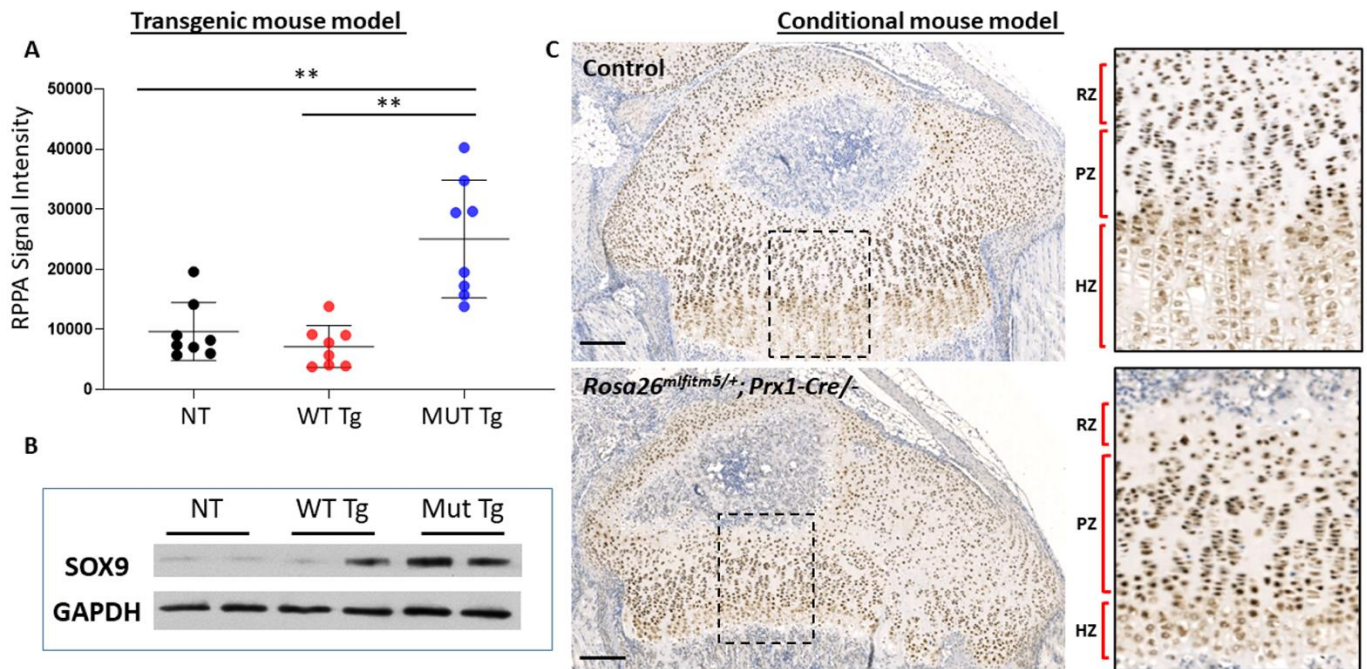
2 **Fig. 7: Expression of the mutant *Ifitm5* allele leads to altered spatio-temporal expression of**

3 **SOX9.** (A) RPPA in transgenic *Ifitm5$^{c.-14C>T}$* mouse model. SOX9 RPPA signal intensity is

4 increased in calvaria protein extract from mice overexpressing mutant *Ifitm5* (MUT Tg), as

5 compared to mice overexpressing wild type Ifitm5 (WT Tg), and non-transgenic (NT) littermates

6 (n=8 per group, one-way ANOVA with Tukey's post-hoc tests, all comparisons to Mut Tg

7 group, **p<0.001). (B) Western blot for SOX9 in representative RPPA samples. (C)

8 Representative immunohistochemistry images of proximal tibia of control (top) and mutant

9 (*Rosa26$^{mIfitm5/+}$;*Prx1-Cre/-, bottom) mice at age 2 weeks, showing increased intensity and altered

10 distribution of SOX9-positive cells in the growth plate. In the mutant mice, SOX9-positive cells

11 are seen throughout the growth plate including the hypertrophic zone (which is reduced

12 compared to littermate controls). Right panel: magnification of insert. RZ= resting zone, PZ=

13 proliferative zone, HZ= hypertrophic zone. Scale bar = 200 um.
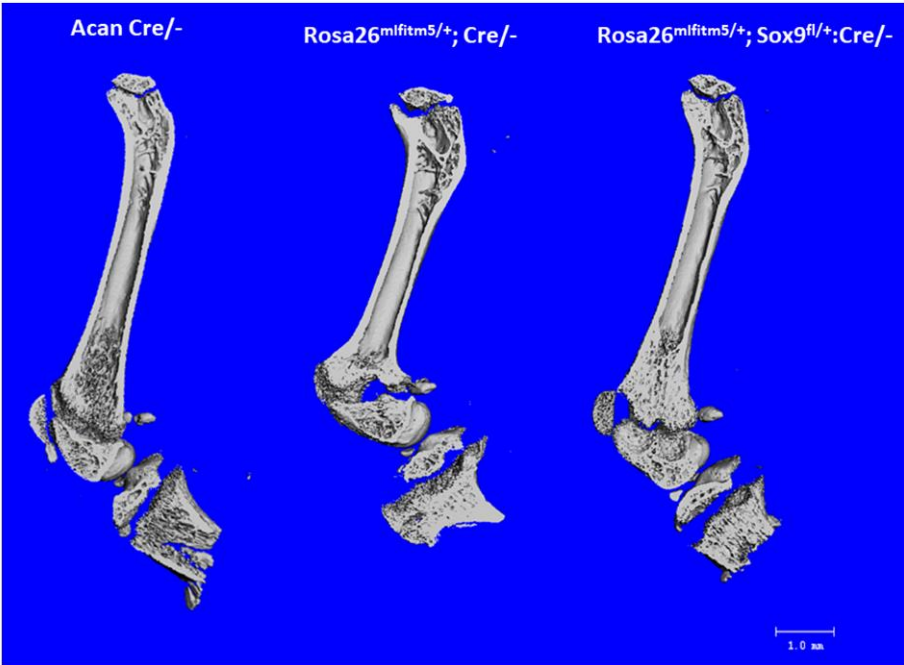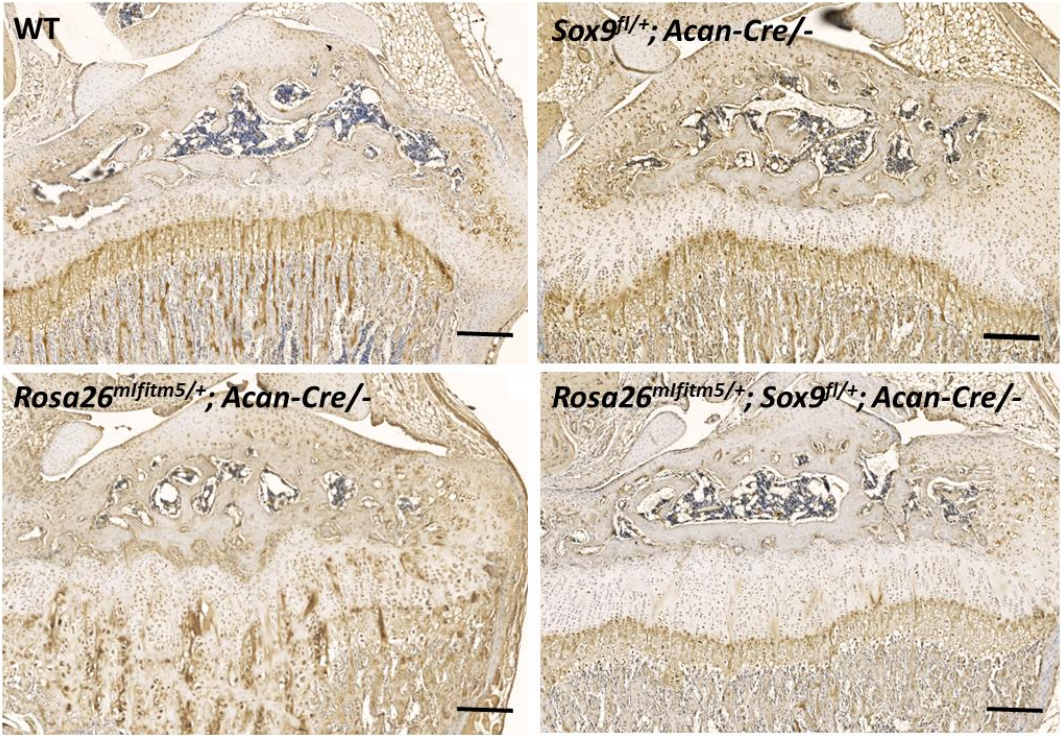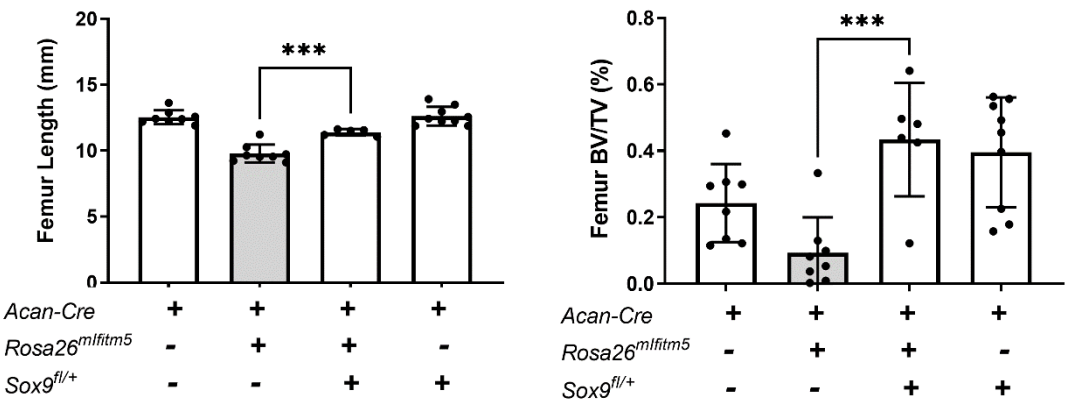
14

1 **Figure 8A-B**

15

29

30

1   **Figure 8C-D**

2

3

16

17
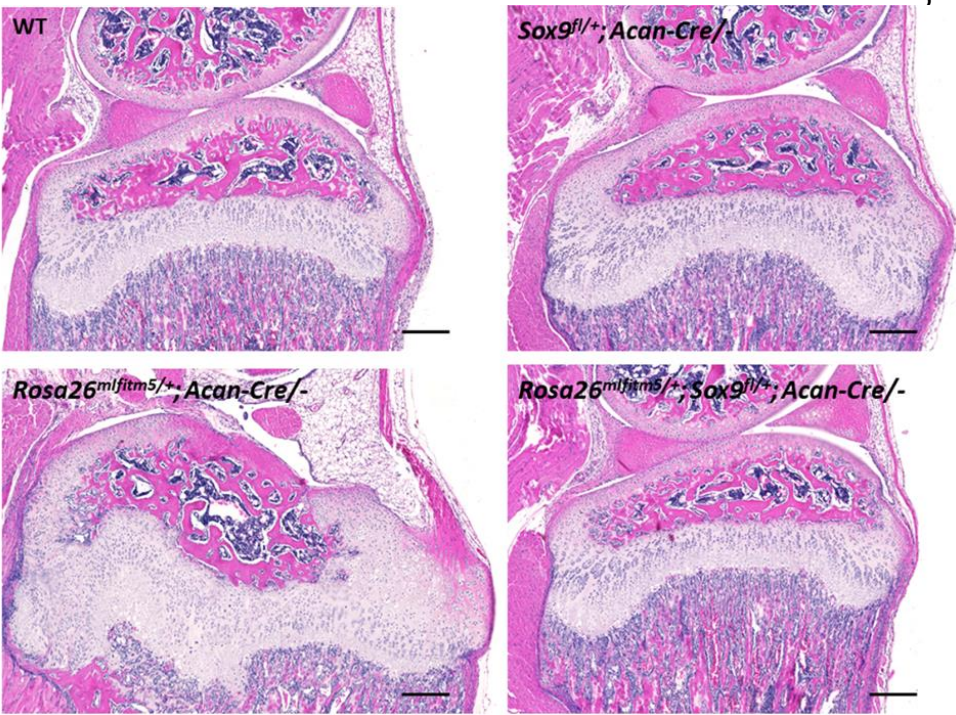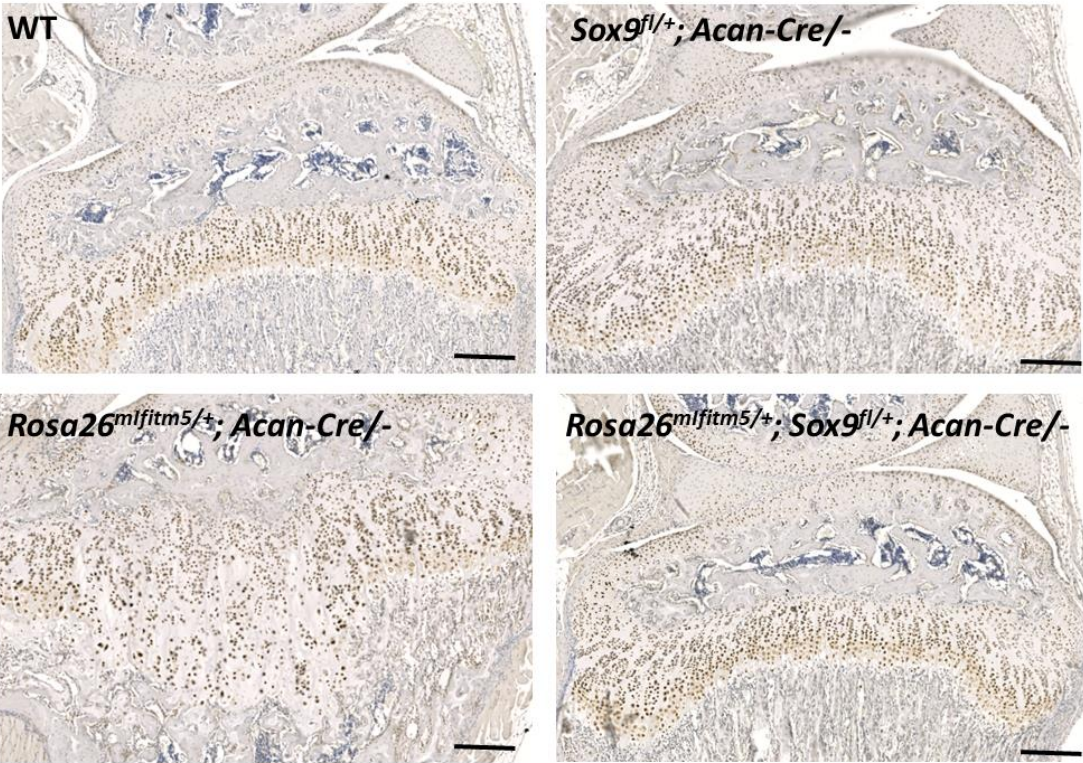
1   **Figure 8E**

9   **Fig. 8: Abnormal skeletal development in *Rosa26^{mIfitm5}*;*Acan-Cre ERT2* mice is**

11   **partially rescued by *Sox9* deletion.** (A-C) Histology sections of

12   *Rosa26^{mIfitm5/+}*;*Acan-Cre* ERT2 mice, showing disrupted growth plate architecture caused by

13   post-natal activation of mutant *Ifitm5* in chondrocytes (left panel, bottom), while *Sox9* deletion

14   (right panel, bottom) rescued the growth plate structure. Hematoxylin & Eosin (A) and

15   immunohistochemistry for SOX9 (B) and type X collagen (C), Scale bar=200 uM. (D) Growth

16   delay in *Rosa26^{mIfitm5/+}*;*Acan-Cre* ERT2 mutant mice (middle), compared to wild type (left) and

17   partial rescue by *Sox9* deletion (right). (E) Micro-CT analysis of femur length (left) and BV/TV

18   (right) in *Rosa26^{mIfitm5/+}*;*Acan-Cre* ERT2 mice, showing low bone mass in mutant mice, and

19   partial rescue by *Sox9* deletion (one-way ANOVA, n=6-8 per group, ***p=0.0005). For all

20   experiments shown, *Cre* recombinase was activated by intraperitoneal tamoxifen injections (10

21   mg/kg/dose) at P.10-15 and samples collected at age 5 weeks.

22

23

24

25

1   **Figure 9A-B**

2

3
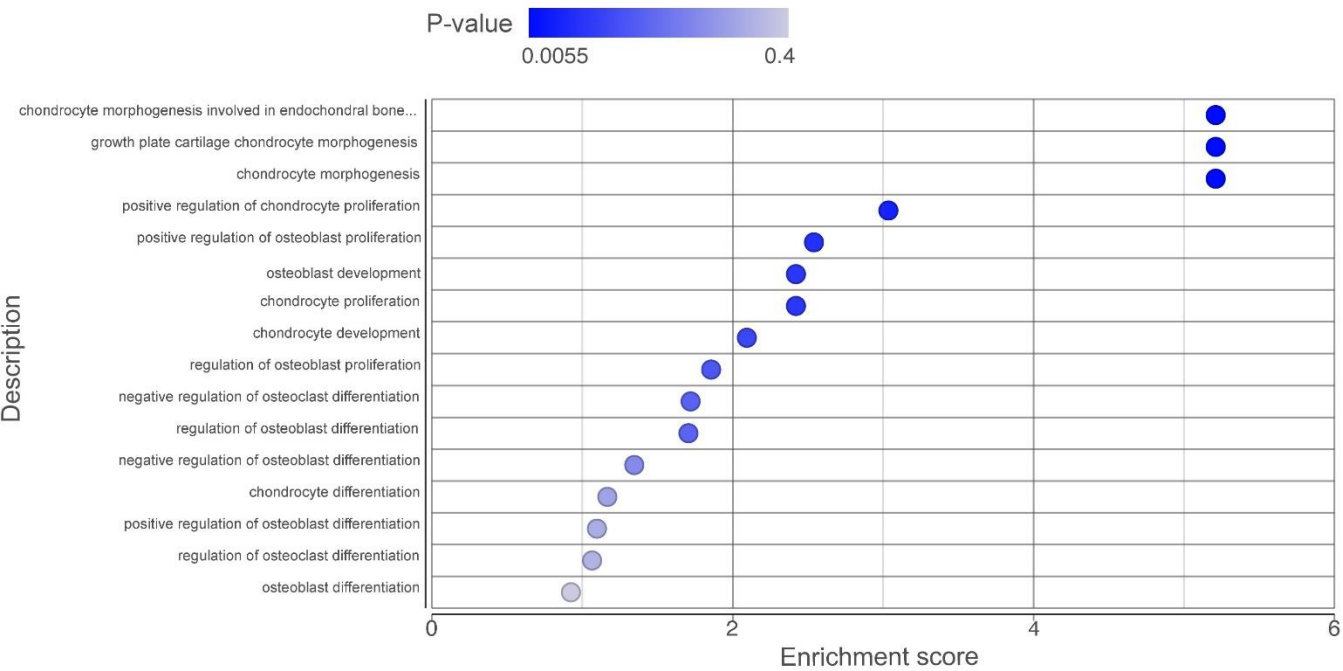
4

5

6

7

8

9

10

11

12

13

14

15

16

17

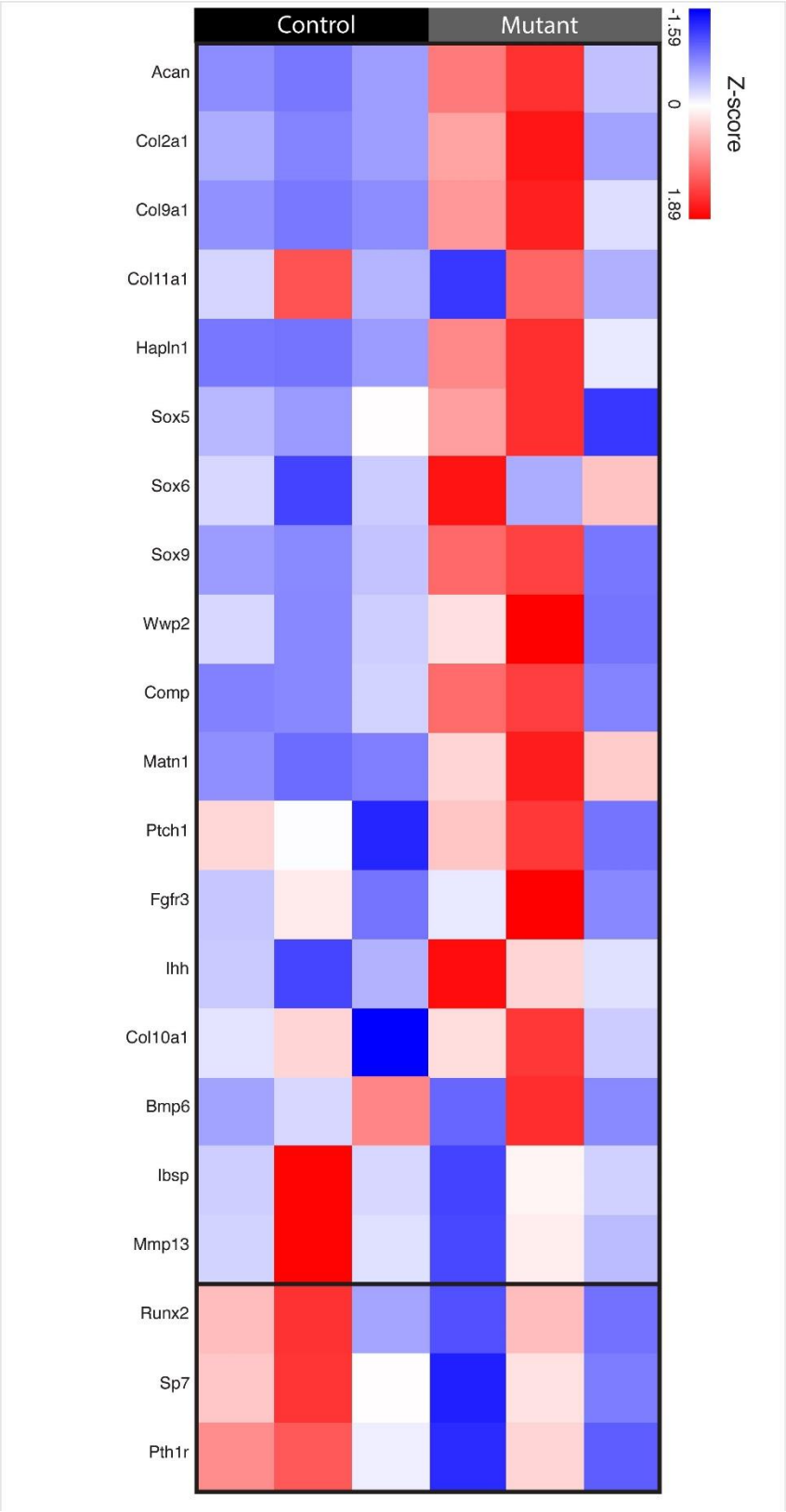18
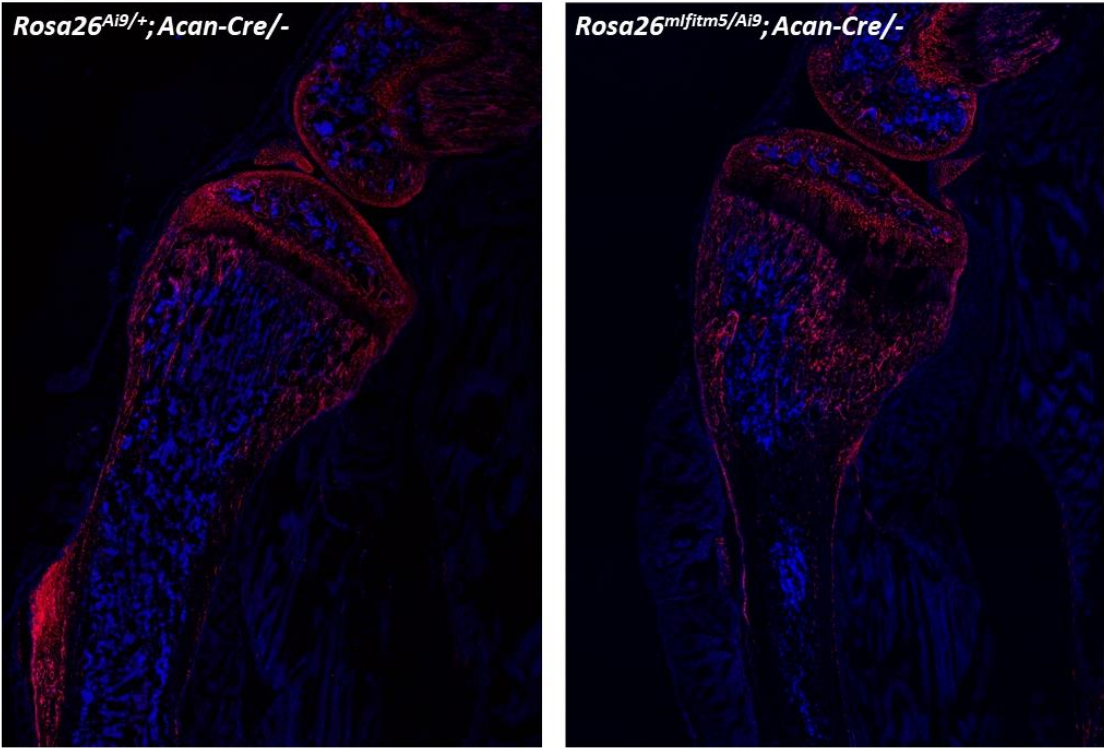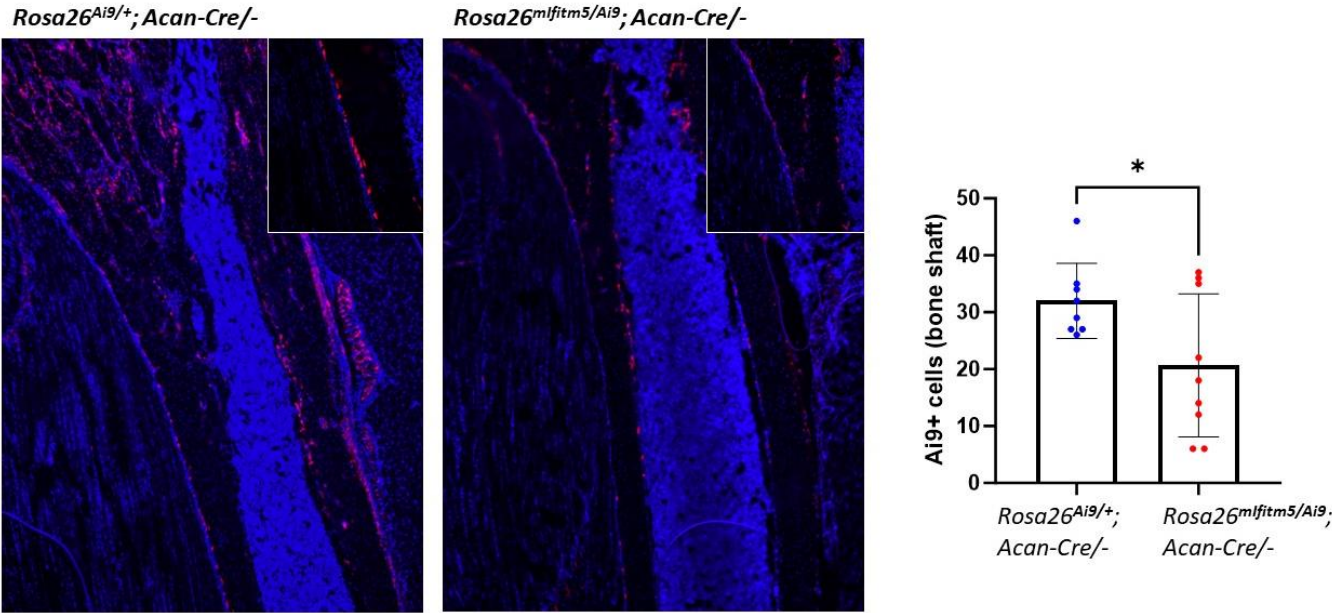
1 **Figure 9C**

C

4
5
6
7
8
9
10
11
12
13
14
15
16

Figure 9D

1 **Fig. 9: Expression of the mutant *Ifitm5* allele leads to altered skeletal stem cell**

2 **differentiation and enhanced chondrogenesis**. (A-B) Lineage tracing of chondrocytes co-

3 expressing mutant *Ifitm5* and Ai9 reporter in *Rosa26$^{mIfimt5/Ai9}$;Acan-Cre ERT2* mice. Tamoxifen

4 induction was performed at postnatal day 10 and bones were collected after 3 weeks (age 5

5 weeks). Representative images of proximal tibia (A) and tibia diaphyseal area (B). Decreased

6 fraction of Ai9+ cells migrated to the bone diaphysis in mutant animals compared to littermate

7 controls (n=3 per genotype, n=2-3 fields counted per sample at x20 magnification, t test

8 *p=0.03). (C) RNA sequencing in total femur cDNA from *Rosa26$^{mIfitm5/+}$;Acan-Cre* ERT2 mice

9 (n=3 per genotype) showed enrichment for chondrogenic gene expression in the mutant samples

10 by GO term analysis. (D) Heat map of focused differential gene expression analysis from RNA

11 sequencing, showing upregulation of chondrogenic gene markers and decreased expression of

12 osteogenic markers in the mutants compared to control group.